

MOUNTAIN-PLAINS CONSORTIUM

MPC 18-352 | P. Powelson, P. Barr, and M. Halling

Long-Term Behavior of Precast Concrete Bridges



A University Transportation Center sponsored by the U.S. Department of Transportation serving the Mountain-Plains Region. Consortium members:

Colorado State University
North Dakota State University
South Dakota State University

University of Colorado Denver
University of Denver
University of Utah

Utah State University
University of Wyoming

Acknowledgments

My sincerest appreciation goes to my supervisor, Professor Paul Barr, for his continuous encouragement, guidance, and support during the entire period of my studies at Utah State University. Without his advice and patience, I would have been unable to complete this thesis. I also wish to express my sincere thanks to the committee members, Dr. Marv Halling and Dr. James Bay, for their advice.

I would also like to thank Shaun Dustin and those from Campbell Scientific Inc. that provided technical assistance with the data collection system. Thanks also to Paul Barr, Marv Halling, and Tyson Alder for their help in installing all of the instrumentation.

Thanks also to my parents for always encouraging me to do my best in my studies. Finally, a very special mention goes to my wife, Lezlie. I would not have been able to complete my studies without her love and continuous support.

Phillip Powelson

LONG-TERM BEHAVIOR OF PRECAST CONCRETE BRIDGES

Phillip Powelson
Paul J. Barr
Marv W. Halling

Utah State University
Department of Civil and Environmental Engineering
Logan, Utah

July 2018

Disclaimer

The contents of this report reflect the views of the authors, who are responsible for the facts and the accuracy of the information presented. This document is disseminated under the sponsorship of the Department of Transportation, University Transportation Centers Program, in the interest of information exchange. The U.S. Government assumes no liability for the contents or use thereof.

NDSU does not discriminate in its programs and activities on the basis of age, color, gender expression/identity, genetic information, marital status, national origin, participation in lawful off-campus activity, physical or mental disability, pregnancy, public assistance status, race, religion, sex, sexual orientation, spousal relationship to current employee, or veteran status, as applicable. Direct inquiries to Vice Provost, Title IX/ADA Coordinator, Old Main 201, 701-231-7708, ndsuoaaa@ndsu.edu.

ABSTRACT

For this research, sensors were used to investigate the differences in prestress losses and temperature gradients in a concrete deck bulb tee girder bridge. The Millville Bridge was built as an access point to the Ridgeline High School in Millville, Utah. The bridge was built in 2016 and presently supports two lanes of traffic.

Changes in prestress were measured with a total of 16 vibrating wire strain gauges located at four cross-sections. Temperature gradients were measured with a total of 50 thermocouples located at five cross-section locations, four of which were shared locations with the vibrating wire strain gauges. These instruments were placed at the mid-span and end of an exterior and center girder to effectively measure the bridge response in one quarter of the bridge superstructure.

The prestress loss recordings were initiated before the prestressing strands were released. The thermocouple data for Girder 1 began to be recorded before the initial casting of the girder concrete. The thermocouple data for Girder 5 was started before the curing blanket was removed in the casting yard. Prestress losses at the girder mid-span and temperature gradients were compared with code recommended values according to the AASHTO bridge design specifications.

TABLE OF CONTENTS

1. INTRODUCTION	1
1.1 Context.....	1
1.2 Research Objectives	1
1.3 Organization of Thesis.....	2
2. LITERATURE REVIEW	3
2.1 Comparison of Prestress Losses for a Prestressed Concrete Bridge Made with High-Performance Concrete	3
2.2 Bridge Prestress Losses in Dry Climate	4
2.3 Design of Concrete Bridges for Temperature Gradients	6
2.4 Temperature Effects on a Box-Girder Integral-Abutment Bridge.....	7
2.5 Measurements of Thermal Gradients and their Effects on Segmental Concrete Bridge	8
3. BRIDGE DESCRIPTION & MEASURED DATA	11
3.1 Bridge Description.....	11
3.2 Instrumentation Plan.....	15
3.3 Prestress Loss Data.....	19
3.3.1 Strain Losses during Initial Destressing	20
3.3.2 Long-Term Strain Losses	25
3.4 Temperature Data	27
3.4.1 Curing Temperature Data	27
3.4.2 Temperature Gradients during Curing.....	28
3.4.3 Long-Term Temperature Data.....	29
3.4.4 Long-Term Temperature Gradients.....	33
3.4.5 Long-Term Temperature Gradients for Site E.....	35
4. COMPARISON WITH PREDICTIVE METHODS.....	37
4.1 Description of AASHTO Short-Term Losses.....	37
4.2 Description of AASHTO LRFD Long-Term Losses Using the Refined Method	38
4.3 Description of AASHTO Approximate Method.....	39
4.4 Comparison of Predictive Methods with Measured Losses.....	39
4.4.1 Predicted Elastic Shortening Loss Comparison.....	39
4.4.2 Predicted Long-Term Losses Using Equation 4.3 Comparison.....	40
4.4.3 Predicted Long-Term Losses Using Equation 4.4 Comparison.....	40
4.5 Description of AASHTO Temperature Prediction	41
4.6 Comparison of AASHTO Temperature Prediction with Measured Temperatures.....	42

5. SUMMARY AND THESIS.....	46
5.1 Summary.....	46
5.2 Conclusions	46
5.3 Recommendations for Additional Research	47
BIBLIOGRAPHY	48
APPENDIX A.....	49

LIST OF TABLES

- Table 2.1 Lifetime Creep and Shrinkage Losses 5

- Table 3.1 Comparative Concrete Strengths 20
- Table 3.2 Elastic Shortening Loss Comparison at Mid-span for Girder 1 and Girder 5..... 21
- Table 3.3 Loss Reductions Due to Friction in Casting Bed..... 23
- Table 3.4 Calculated Friction Force in Casting Bed..... 23
- Table 3.5 Strain Losses Due to Yard Girder Picking Points..... 23
- Table 3.6 Worst Case Temperature Gradients Information 28
- Table 3.7 Worst Case Temperature Gradients Information 33
- Table 3.8 Worst Case Temperature Gradient Information for Site E 35

- Table 4.1 Elastic Shortening Comparison..... 39
- Table 4.2 Long-Term Loss Comparison Using Equation 4.3 40
- Table 4.3 Long-Term Loss Comparison Using Equation 4.4 40
- Table 4.4 Bridge Temperature Gradient Specifications..... 41

- Table 5.1 Long-Term Percent Errors of Refined and Approximate Methods Using AASHTO and
ACI Modulus of Elasticity Equations 47

LIST OF FIGURES

Figure 3.1	View of Millville Bridge.....	11
Figure 3.2	Bridge Cross-Section (dimensions given in meters).....	12
Figure 3.3	Harped Strands Diagram.....	12
Figure 3.4	Girder Dimensions (dimensions are given in mm).....	13
Figure 3.5	Girder in the Casting Bed at the Prestress Yard.....	13
Figure 3.6	Millville Bridge Diaphragm.....	14
Figure 3.7	Millville Bridge Abutments.....	15
Figure 3.8	Instrumentation Site Layout Plan (Dimensions in meters).....	16
Figure 3.9	Typical Instrumentation Site.....	17
Figure 3.10	Typical Girder Instrumentation Plan (Dimensions in mm).....	18
Figure 3.11	Typical Bank of Thermocouples.....	19
Figure 3.12	Strain Losses during Bridge Initial Destressing.....	20
Figure 3.13	Increases in Strain Losses Due to Transporting Girder from Bed to Yard.....	22
Figure 3.14	Linear Regression Example Used for Friction and Picking Points Loss Calculations.....	22
Figure 3.15	Initial Girder Destressing Strain Losses for Site A.....	24
Figure 3.16	Initial Girder Destressing Strain Losses for Site B.....	25
Figure 3.17	Long-Term Prestressing Steel Strain Losses at Mid-Span for Girder 1.....	26
Figure 3.18	Long-Term Prestressing Steel Strain Losses at Mid-Span for Girder 5.....	26
Figure 3.19	Long-Term Prestressing Steel Strain Losses at Mid-Span for Girders 1 and 5.....	27
Figure 3.20	Girder 1 Temperatures during Curing.....	28
Figure 3.21	Maximum Temperature Gradient during Curing Using the Difference between Thermocouples 1 and 10.....	29
Figure 3.22	Minimum Temperature Gradient during Curing Using the Difference between Thermocouples 1 and 10.....	29
Figure 3.23	Girder 1 Long-Term Temperatures.....	30
Figure 3.24	Girder 1 VWSG Temperatures at Mid-Span.....	30
Figure 3.25	Girder 5 Long-Term Temperatures.....	31
Figure 3.26	Girder 5 VWSG Temperatures at Mid-Span.....	31
Figure 3.27	Girder 1 Temperatures during Abutment Casting.....	32
Figure 3.28	Girder 5 Temperatures during Abutment Casting.....	32
Figure 3.29	Maximum Long-Term Temperature Gradient.....	33
Figure 3.30	Minimum Temperature Gradient during Girder Cooling.....	34
Figure 3.31	Minimum Long-Term Girder Temperature Gradient.....	34
Figure 3.32	Maximum Long-Term Temperature Gradient at Site E.....	35
Figure 3.33	Minimum Long-Term Temperature Gradient at Site E.....	36
Figure 4.1	Mid-Span Stress Loss Comparisons.....	41
Figure 4.2	3.12.3-2 of the AASHTO LRFD Bridge Design Specifications.....	42
Figure 4.3	Maximum Positive Temperature Gradient Comparison.....	42
Figure 4.4	Minimum Temperature Gradient Comparison.....	43
Figure 4.5	Site E Maximum Temperature Gradient Comparison.....	44
Figure 4.6	Site E Minimum Temperature Gradient Comparison.....	44

1. INTRODUCTION

1.1 Context

Several studies have been performed focusing on prestress losses and temperature gradients for various kinds of bridges and concretes. For example, Barr, Kukay, and Halling (2008) examined the bridge prestress losses for a multi-span prestressed concrete bridge made with high-performance concrete. Saiidi, Hutchens, and Gardella (1998) studied bridge prestress losses in a dry climate. For these and other studies, conventional bridges with cast-in-place decks were monitored. Precast deck bulb tee girders provide an efficient cross section for ABC construction. However, few bridges of this type have been studied.

The Utah Transportation Center (UTC), located on the campus of Utah State University (USU), in partnership with the Mountain Plains Consortium (MPC), sponsored a study to investigate the differences in prestress losses and temperature gradients calculated according to the AASHTO LRFD Bridge Design Specifications and measured values obtained from vibrating wire strain gauges and thermocouples placed at five different locations in a concrete deck bulb tee girder bridge. The bridge was instrumented with 16 vibrating wire strain gauges with integral thermistors located at four cross-sections. Additionally, 50 thermocouples were placed at five cross-section locations, four of which were shared locations with the vibrating wire strain gauges. These instruments were placed at the mid-span and end of an exterior and center girder to effectively measure the bridge response in one quarter of the bridge superstructure. These instruments were placed in the precast plant and tied to the reinforcing steel before the concrete was poured.

The prestress loss recordings were initiated before the prestressing strands were released. The thermocouple data for Girder 1 began to be recorded before the initial casting of the girder concrete. The thermocouple data for Girder 5 were not recorded during casting and curing of the girder concrete, but started before the curing blanket was removed in the casting yard. All data were recorded until February 29, 2016. Prestress losses at the girder mid-span and temperature gradients were compared with code recommended values according to the AASHTO bridge design specifications.

1.2 Research Objectives

This research compared the prestress losses and temperature gradients calculated according to the AASHTO LRFD specifications to the measured results on a bridge made with precast deck bulb tee girders. Additionally, prestress loss effects from the friction in the casting bed and from lifting the girder by the lifting loops cast into the concrete were monitored. The friction and picking points' losses were shown as a sudden increase in strain loss when the girder is released from the bed and a sudden decrease in strain after the girder is placed in the yard and the support conditions changed.

The AASHTO LRFD specifications provide an approximate method for calculating a long-term prestress loss estimate, and a refined method for calculating the prestress losses at any time during the life of the bridge. The AASHTO LRFD specifications also provide the method to estimate the maximum and minimum temperature gradient based on the region of the country and type of bridge. The Priestley (1978) proposed maximum temperature gradient was also used to compare against the measured temperatures.

The objective of this research was to monitor actual behavior of the deck bulb tee bridge girders during curing and while in service. The behavior of these girders can then be compared with predictive methods according to current design standards. Differences can be quantified and recommendations can be provided to more accurately predict bridges of this type.

1.3 Organization of Thesis

The research data for this thesis are organized in this manner:

- Section 2 presents a review of previous studies relating to prestress losses and temperature gradients
- Section 3 provides details of the bridge specifications, instrumentation plan, measured data, and behavior
- Section 4 compares the results of the measured data with predictive methods according to current design methodologies
- Section 5 provides a summary of the research, conclusions, and recommendations for future work

2. LITERATURE REVIEW

This section reviews some of the previous research performed by other professionals in this field and the conclusions they reached.

2.1 Comparison of Prestress Losses for a Prestressed Concrete Bridge Made with High-Performance Concrete

P.J. Barr, B.M. Kukay, and M.W. Halling (2008)

Researchers at Utah State University analyzed the effects of using high performance concrete (HPC) on the prestress losses of the SR18/SR516 overcrossing in Washington. By utilizing HPC, the Washington State Department of Transportation (WSDOT) was able to reduce the necessary number of girders from seven to five. Test results from these HPC prestressed girders were compared to methods for calculating prestress losses, namely by the American Association of State Highway and Transportation Officials (AASHTO 2004 and National Cooperative Highway Research Project [NCHRP] 18-07).

The researchers embedded vibrating-wire strain gauges with integral thermistors in three long-span and two short-span girders. These gauges monitored concrete temperature and longitudinal strains at two sites in each girder that were near the mid-span and the end nearest a support pier. The researchers placed the gauges at the centroid of the prestressing steel strands. The data logger recorded changes in behavior for three years, beginning at the time of casting. The gauges were monitored every 15 minutes during curing, every hour during destressing, and every six hours after six months.

Due to prestress losses, the prestressing force in a girder during service is less than at initial stressing. Using vibrating-wire strain gauges, the researchers measured the change in strain in the prestressing strands using the following equation to calculate the change in stress:

$$\Delta f_{pPL} = E_p * \Delta \epsilon_c \quad \text{Equation 2.1}$$

Where: Δf_{pPL} = change in steel stress due to prestress losses; E_p = modulus of elasticity of prestressing steel (28,500 ksi); and $\Delta \epsilon_c$ = measured change in strand strain. The measured strains in the prestressing strands were averaged and used with Equation 2.1 to determine the prestressing losses. These losses were compared with the prestress losses predicted by applying the AASHTO LRFD and the NCHRP 18-07 methods. The prestress losses calculated according to the AASHTO LRFD were higher for both the long- and short-span girders than the losses calculated according to the NCHRP 18-07 method. The calculated AASHTO prestress losses for the long span at nearly three years were 20% higher than the average measured prestress loss. In contrast, the NCHRP 18-07 method's calculated losses were about 22% less than the measured losses. For the short span, the AASHTO LRFD method was within 2% of the measured losses and the NCHRP 18-07 method was 22% less than the measured losses. In order to investigate the sources of the discrepancies, the measured and predicted prestress losses were compared in the three major prestress loss components of elastic shortening, creep and shrinkage, and differential shrinkage. Elastic shortening occurs when the prestressing strands are released and the force in the strands is transferred to the bonded concrete, causing the concrete to shorten under the applied load. These losses were estimated by measuring the change in strain of the concrete at the centroid of the prestressing strands once the strands were released and multiplying this strain by the modulus of elasticity of the prestressing strands (Equation 2.1). In comparing the measured elastic shortening losses to the predicted losses, the researchers found that the AASHTO LRFD method underpredicted the elastic shortening losses for both the short and large spans. The measured elastic shortening losses were about 3% smaller and 5% larger than the NCHRP 18-07 for the long and short span, respectively.

Loss due to creep and shrinkage is time dependent and was calculated by subtracting the elastic shortening loss from the total prestress losses. After three years, the AASHTO LRFD creep and shrinkage loss was 42% larger than the average measured losses for the long span. Also, for the long span, the NCHRP predicted creep and shrinkage losses to be 30% smaller than the measured losses. For the short span, the AASHTO LRFD creep and shrinkage losses were within 12% while the NCHRP losses were nearly 40% smaller than the measured losses. This large difference for the NCHRP losses was assumed to be due to the smaller stress that was applied to the shorter span girders. The NCHRP method was developed based on lower creep and shrinkage values for high-performance concrete.

The differential shrinkage loss occurs after the deck is placed (typically a few months after the girder concrete has already been cast). At this time, the rate of creep and shrinkage of the girder has slowed significantly, and the deck concrete is just beginning to experience shrinkage. Differential shrinkage refers to the effect of differences between the shrinkage strain of the deck concrete and the girder concrete. The AASHTO LRFD method does not explicitly take into account the effect of differential shrinkage; therefore, using the NCHRP 18-07 method, the researchers found the girders to behave as though they were partially restrained at the supports. Using this, the researchers concluded that the average prestress loss, due to differential shrinkage, was close to the predicted loss of a continuous beam (within 1 ksi).

The researchers concluded that with a measured elastic modulus and by analyzing the girders as continuous beams, the NCHRP 18-07 method would have been within 10% of the measured prestress losses. When the same calibrated elastic modulus was used in the AASHTO LRFD method, the predicted losses would have been over 30% higher than the measured losses. The AASHTO LRFD method was closer, however, for the short span girders due to the lower applied stress. Also, the variations in individual prestress loss components are believed to have been significantly influenced by curing. Finally, the NCHRP method was closer to estimating the elastic shortening than the AASHTO LRFD method, and the SR18/SR516 bridge behaved as a partially continuous bridge at the time of deck casting.

2.2 Bridge Prestress Losses in Dry Climate

M. Saiidi, E. Hutchens, D. Gardella (1998)

Researchers from University of Nevada, Reno measured and analyzed the prestress losses for a post-tensioned, simply supported, box-girder bridge in southern Nevada. Specifically, the study was performed to investigate the potential adverse effects of low relative humidity (RH) on prestress losses. Measured prestress forces and deflection were monitored over a 24-month period, and predictions were calculated in accordance with the (1) American Association of State Highway Transportation Officials (AASHTO) specifications (1992), (2) American Concrete Institute (ACI) Committee 209, (3) Prestressed Concrete Institute (PCI) Committee report, and (4) Naaman's time-step method.

The researchers instrumented the bridge with 12 electrical strain gauges that were bonded to the prestressing steel, four mechanical strain gauges that were attached to the girder webs, and two temperature gauges that were mounted near the instrumented area. For prestressing losses, the majority of the losses occur early in the life of the bridge. Therefore, the measurement schedule was as follows: once per day for the first week, at the end of two weeks, once per month through the first six months, and at two-month intervals through the following 18 months. On each collection day, measurements were taken hourly from the strain gauges for a 24-hour period to obtain the average throughout the day.

The change in tendon stresses excluded the immediate losses due to elastic shortening, friction, and anchorage set. Elastic shortening and friction were calculated using the AASHTO specifications;

anchorage set was found based on Naaman (1982). All other measured prestress losses were assumed to be from creep and shrinkage.

The researchers found that the difference between the ambient temperature data and the measured bridge temperature data was typically between 2°F and 3°F. The temperature and RH data results generally showed opposite trends, one would increase as the other decreased. All stress data from the electrical and mechanical strain gauges showed similar trends with no pronounced difference. The results from the stress data showed that during periods of high relative humidity, the prestress loss rate slowed. As the temperature increased and relative humidity decreased, the loss of moisture in the bridge led to shrinkage of concrete, and subsequently, higher prestress loss rates.

The center span deflection of the bridge was also measured. The data showed that when the tendon force was nearly constant or rising, the bridge generally deflected upward. The opposite occurred as the prestress force decreased. The deflection results were compared with the Nilson (1987) Method and a close correlation was found between the measured and calculated data results.

Four methods were used to estimate the prestress losses: (1) the AASHTO (1992) specifications, (2) the Naaman (1982) Method, (3) the ACI Committee 209 recommendations, and (4) the PCI recommendations (PCI 1975). The PCI method does not account for RH explicitly. The other three methods assume a constant average ambient RH. The effects of variable temperature and humidity were included in the analysis of the actual data and in the theoretical analysis. To compare lifetime losses, a regression analysis of the measured tendon losses was matched with a logarithmic fit, and the loss was determined at 40 years.

Table 2.1 Lifetime Creep and Shrinkage Losses

Method	Creep (ksi)	Shrinkage (ksi)	Total (ksi)
AASHTO (1992)	15.1	10.6	25.7
Naaman (1982)	11.4	7.1	18.5
ACI Committee 209	10.1	8.9	19.0
PCI Committee (1975)	5.3	10.0	15.3
Extrapolated Measured Data	NA	NA	18.1

Table 2.1 shows the comparison made between the four different methods with the measured extrapolated data. The data show that the PCI (1975) method is about 15% lower than the extrapolated data, which the researchers attributed to the fact that the method does not treat RH as a parameter.

The researchers concluded that the extrapolated measured creep and shrinkage prestress losses were approximately 30% lower than the estimated values calculated using the AASHTO method. Also, the AASHTO method was conservative by approximately 20% at predicting the total losses (excluding elastic shortening). It was, therefore, recommended to the Nevada Department of Transportation (NDOT) to continue to design prestress concrete bridges in southern Nevada using the AASHTO method. For northern Nevada, due to high daily and seasonal variation of RH, an additional study was being performed. The researchers also found that the Naaman (1982) and ACI Committee 209 methods showed a very close correlation. The PCI method led to considerably lower losses than the measured losses and does not explicitly account for the effect of low RH on site. Therefore, the researchers recommended the ACI 209 and Naaman (1982) methods for use in more accurate calculation of creep and shrinkage losses. Finally, the data from a logarithmic fit of the measured deflections showed good agreement with the predicted values from the equation presented by Nilson (1987).

2.3 Design of Concrete Bridges for Temperature Gradients

M.J.N. Priestley (1978)

Priestley performed a study to analyze the bridge response to temperature gradients. Previously, engineers designed bridges to account for longitudinal movements induced by temperature changes of $\pm 36^\circ\text{F}$. This was accomplished through specifying sliding joints, bearing displacements, or a flexible pier design. Priestley studied the effects of temperature gradients in response to severe cracking of Auckland, New Zealand's, New Market Viaduct.

First, Priestley analyzed methods to predict the critical design gradient based on known local ambient characteristics. To describe the thermal response of the bridge, the Fourier conduction equation was used. However, the solution for said equation with the given boundary condition is impossible. To be able to analyze the section, transverse heat flow was assumed to be negligible, simplifying the equation such that the section can be analyzed by finite element methods. To analyze the thermal response of a complex section, the section was analyzed for several cross-sections and combined to produce the total results for the section.

Second, stress levels induced in the bridge superstructure by the design thermal gradient were calculated. Using principles of thermal expansion and the Navier-Bernoulli hypothesis, Priestley proposed the following equation for the internal moment induced by the temperature gradient:

$$M = E \int (\varepsilon_{(y)} - \alpha t_{(y)}) b_{(y)} (y - n) dy \quad \text{Equation 2.2}$$

Where: M = moment on cross-section, E = concrete modulus of elasticity, $\varepsilon_{(y)}$ = final strain profile, α = linear coefficient of thermal expansion, $t_{(y)}$ = vertical gradient of temperature change, $b_{(y)}$ = net section width at height y , and n = location of neutral axis. To compare the theoretical stresses to actual stresses, a model was subjected to simulated ambient temperature and radiation intensity variation with an environmental box. The results of the experiment showed good agreement with the predicted values. The design thermal gradients depend on ambient temperature, incident solar radiation levels, and the average wind speeds. If the bridge has an asphalt topping, the effect is similar to a thermal insulator, causing the thermal gradient to lower. The following equation has been proposed:

$$t_y = T \left(\frac{y}{1200} \right)^5 \quad \text{Equation 2.3}$$

Where: $t_{(y)}$ = vertical gradient of temperature change, T = maximum temperature at the deck surface, and y = depth (in mm) from deck surface.

Finally, Priestley assessed the significance of the thermally induced stresses to serviceability and ultimate load characteristics. For normal reinforced concrete bridges, substantial cracking will have occurred under dead plus live load prior to thermal loading. Also, levels of reinforcement stress due to thermal loading are unlikely to cause fatigue problems. For prestressed concrete bridges, a feasible design approach would be to ignore thermal loading and rely on the reduction in flexural rigidity on cracking, as with normal reinforced concrete. For the specific situation where the prestress overbalances the dead load, large sagging moments at the internal support can occur and can cause cracking if a thermal gradient is applied. As temperature causes a deformation and not a force directly, the ultimate effect of thermal loading on a concrete bridge can be misunderstood. The thermal load effect was found by calculating the thermal deformation and finding the equivalent force. The same would apply for the ultimate load, which is multiplying the thermal deformation by a 1.7 factor and finding the equivalent force.

Priestley concluded the following:

- Thermal fluctuations can induce substantial stress in continuous bridge superstructures.
- Good agreement was shown between theoretical and experimental measurements, enabling thermal effects to be accurately estimated.
- Partial prestressing to reduce thermal stress levels may be a viable design option, though more research would be required.
- Thermal effects are generally insignificant when analyzing ultimate load and only need to be considered for serviceability checks.

2.4 Temperature Effects on a Box-Girder Integral-Abutment Bridge

L.E. Rodriguez, P.J. Barr, M.W. Hallan (2014)

The researchers used changes in measured temperature to obtain maximum and minimum average temperatures as well as positive and negative thermal gradients for a bridge near Elk Grove, California. The maximum and minimum average temperatures were compared with the AASHTO LRFD 2010 method. Additionally, maximum and minimum temperature gradients were compared with AASHTO 1994 & 2010 and the Priestly 1978 methods. Changes in strain at various locations obtained by driving trucks along five load paths were used along with strain changes from daily temperature variations to validate a finite-element model of the bridge. This model was used to evaluate the effects that the existing partial fixity and temperature gradients have on the temperature induced stress for the bridge.

The bridge used in this study is part of the Interstate 5 (I-5) corridor crossing over Lambert Road and was completed in 1975. This bridge is a cast-in-place, post-tensioned, box-girder bridge with two equal spans of 129 feet. The bridge was designed as live-load continuous. To quantify the overall response from changes in temperature, a number of tilt meters, thermocouples, and vibrating wire strain gauges were installed on the bridge superstructure. A total of 46 thermocouples were installed. Twelve were placed on the outside concrete surface at the bottom of the web of girders. An additional four were placed on the concrete surface at the top web of the middle girder and five on an exterior and interior web surface of two girders. Finally, two groups of 10 thermocouples were placed in the bridge deck. Several thermocouples of the two groups of 10 were placed in the top part of the deck where most of the temperature gradient occurs. The researchers monitored the temperature response for one year using this dense array of thermocouples. Changes in concrete temperature were recorded to find the maximum and minimum average values on a daily basis and daily temperature gradients.

During the one-year study, all average daily temperatures were within the maximum and minimum AASHTO LRFD design temperatures, although they did approach the maximum design temperature (within 6°F in July 2011). The maximum positive and negative temperature gradients were found by using the girder web temperatures as a baseline and subtracting these temperature values from the deck temperatures.

For this study, the maximum positive and negative temperature gradients found were 43°F and -16°F, respectively. The majority of the temperature gradient results were less than both the AASHTO 1994 & 2010 and Priestly 1978 methods, the exception being the maximum negative temperature gradient at the bottom of the girder that was three times larger than either of the design gradients. Inasmuch as a negative temperature gradient at the bottom of the girder would decrease the tensile stress, the design was still concluded to be conservative. The researchers developed a finite-element (FE) model to quantify the effect of temperature gradients on continuous, integral-abutment bridges.

As part of the study, a live-load test was performed to validate the FE model. Five predetermined load paths were used to maximize the moment for various girders. The researchers validated the FE model by

comparing the FE predicted strain values to the measured values. The results of the test determined the partial fixity of the bridge, and the effects of temperature could be estimated. The strains from the live-load test were predicted to within 5%, and strains from daily temperature variation were predicted to within 14% of actual measured values. The FE model also showed that the maximum temperature-induced strains are larger than the strains measured during the live-load test.

Finally, the study found that for the Lambert Road Bridge, an under-conservative tensile stress increase of 18% was obtained over the height of the web in comparison with the validated FE model if the assumed design condition of pinned-roller boundary condition were applied. These tensile stresses were still conservative, however, and represented 59% of the allowable tensile stress of a structure per the AASHTO LRFD Specifications (2010). The partial fixity reduced the tensile stress at the bottom of the girder to 44% of the assumed design conditions, helping to reduce this design constraint.

2.5 Measurements of Thermal Gradients and their Effects on Segmental Concrete Bridge

C.L. Roberts-Wollman, J.E. Breen, J. Cawrse (2002)

The researchers at Virginia Polytechnic Institute and State University measured the thermal gradients and their effects on a segmental concrete bridge. The project, known as the San Antonio “Y” project, was an extensive upgrade project to the intersection of interstate highways I-35 and I-10. Temperature measurements were recorded throughout the depth of the segmental concrete box-girder bridge. The maximum recorded positive and negative thermal differentials were reported and compared with current design recommendations. The researchers also analyzed the measured bridge temperatures and the ambient climatic conditions as recorded by the National Weather Service. Equations were then developed to predict positive temperature differentials. Finally, the predicted response of the bridge to positive thermal gradients was quantified.

The peak positive temperature gradients were found to be the difference between the top thermocouple and the coolest web thermocouple. This information was recorded with and without two inches of asphalt topping and compared with the AASHTO (1994a) LRFD specifications and the AASHTO (1999) segmental guide specifications. The researchers concluded that for both surface conditions, the measured gradients were smaller than the design gradients.

Next, the researchers compared the measured temperatures through the depth of the bridge for many days and compared the results with the following equation proposed by Priestley (1978):

$$T(y) = T \left(\frac{y}{1200} \right)^5 \quad \text{Equation 2.4}$$

Where: $T(y)$ = temperature at depth y below top surface; T = temperature at surface; and y = depth below top surface (mm). After comparing the measured temperatures with the fifth-order curve predicted temperatures, the researchers noted several patterns, namely:

- For several days, the measured temperatures near the top surface dropped off more quickly with depth than a fifth-order curve. This distribution occurred on days of high solar radiation after several days of very little sunshine.
- Days that the temperature distribution followed the fifth-order curve occurred on days when the climatic conditions were relatively uniform. This temperature profile was most common.
- Several sets of readings deviate significantly from the fifth-order curve. These sets occur on days of very low sunshine due to the passage of a cool or cold front.

The researchers concluded that the majority of days corresponded closely with the fifth-order curve and that the coolest web temperature typically occurred at 48 inches (1220 mm) below the top surface of the deck. Based on these observations, the researchers extrapolated the deck surface temperature difference using Eq. 2.5.1. The study found that the actual measured differences were well below the design values. The researchers found that the peak negative temperature differences were less than the AASHTO (1994b) LRFD, but slightly greater than the AASHTO (1999) segmental specifications. The shapes of the measured gradients were found to be similar to the design gradients near the deck, but quite different toward the bottom of the girder. As with the positive gradient, the researchers extrapolated to calculate the top surface temperature. The data indicated the AASHTO LRFD recommendations were conservative for all measured days. The AASHTO segmental specification gradient was conservative for all but 12 of the 212 days without asphalt topping and conservative for all but 20 of the 446 days with a two-inch asphalt topping.

Next, the team analyzed methods for predicting the magnitude of the positive temperature difference. The required ambient climatic information was obtained from the National Weather Service observation station, approximately six miles away. These data included daily high and low ambient temperatures, daily average wind speed, and percent possible sunshine. The researchers used this information and the equations presented by Duffy and Beckman (1980) to calculate the theoretical solar radiation. Using all of this information, the researchers compared the temperature differences predicted by Potgieter and Gamble (1983) with the measured temperature differences in San Antonio. The study found that the Potgieter and Gamble (1983) method predicts the temperature difference trends rather well, but the calculated magnitudes were much higher than the measured values. The predicted differences were on average 2.8 times the measured difference for the concrete with no topping and 1.5 times the measured difference for the concrete with two-inch asphalt topping.

The researchers examined the relationships between various climatic conditions and resulting bridge temperatures. First, the study found that the coolest web temperature is on average 99.8% the three-day average. Second, the warmest daily deck temperature correlates well with the daily high ambient temperature except in the spring and summer when the higher solar radiation elevates the deck temperature well above the ambient high temperature. Third, the measured daily maximum positive temperature difference follows the same sinusoidal curve as the solar radiation.

From these observations, the researchers modified the Potgieter and Gable (1983) temperature difference equations. The equation was changed from the difference between the high and low ambient temperatures on a given day to the difference between the three-day average temperature and the daily high. This equation was further modified and simplified to only calculate the temperature difference in terms of solar radiation and the daily high minus the three-day average temperature. The resulting equation on average predicted the temperature difference to be 0.6°C lower than the measured difference. All methods studied were shown to work best when weather conditions are relatively stable. All methods were within 1°C of the measured values for the two-inch asphalt topping case, and the proposed simplified equation best predicts the measured values for the no-topping case.

Finally, the researchers performed two studies to measure the bridge response to the daily temperature variations. Temperatures and deflections were read every hour on these occasions. Using the temperature gradients, changes in deflection were calculated by determining the moment that would develop for a fully restrained system. The following equation was used to calculate the induced moment:

$$M = \alpha E \int T(y)b(y)ydy \quad \text{Equation 2.5}$$

Where: $T(y)$ = temperature at distance y from centroid of section; $b(y)$ = width of section at distance y from centroid; y = distance from centroid of section; α = coefficient of thermal expansion ($11 \times 10^{-6}/^{\circ}\text{C}$); and E = modulus of elasticity.

The researchers concluded that the AASHTO (1994) LRFD design temperature gradients were conservative for both the maximum positive and negative cases. The AASHTO segmental gradients were conservative for all positive gradients and conservative for 94% to 96% of the measured negative gradients (94% for no topping case and 96% for the two-inch topping case). The typical positive and negative temperature gradients can be approximated using the Priestley (1978) fifth-order equation. In predicting bridge temperature difference, the coolest web temperature was found to be close to the three-day average ambient temperature, where the highest deck temperature is a function of ambient temperature and solar radiation. Furthermore, the researchers proposed a simplified equation that is more accurate when predicting the positive temperature gradient for the no-topping condition. Finally, if the measured thermal gradient is known, deflections can be predicted quite accurately.

3. BRIDGE DESCRIPTION & MEASURED DATA

3.1 Bridge Description

The bridge instrumented for this study is located in Millville, Utah, approximately 105 km (65 miles) north of Salt Lake City, Utah, and will hereafter be referred to as the Millville Bridge. The study conducted for this project was performed by researchers at Utah State University. The Millville Bridge was designed as a single-span, prestressed deck bulb tee girder bridge with fixed bridge abutments. This bridge was designed to carry two lanes of traffic, one in each direction, and provides an access point for the new Ridgeline High School. The clearance height from the riverbed to the bottom of the girder is approximately 3.41 m (11.5 ft). The bridge will likely incur a very low average daily traffic (ADT). The vast majority of the daily traffic will consist of students' and staff passenger vehicles. There is no skew or super elevation associated with this bridge. Figure 3.1 shows a picture of the bridge.

The overall width of the bridge is 18.3 m (60 ft) measured from outside-to-outside of the barriers and 17.4 m (57 ft. 2 in.) measured from the inside-to-inside of the barriers. The deck is composed of 20.3 cm (8 in.) of reinforced concrete with 5.08 cm (2 in.) of asphalt overlay. The deck was reinforced with steel with a specified yield of 413.7 MPa (60 ksi), size 16 (5) bars with at least a 5.08 cm (2 in.) cover. The girder and deck concrete had a specified compressive strength of 41.4 MPa (6000 psi) at release and 58.6 MPa (8500 psi) at 28 days. Information on critical dates and release information can be found in Table 3.1. The barriers were cast with a cold joint along the plane of the deck and have a height of 1.1 m (3.5 ft) running parallel to the roadway surface. The barriers are reinforced with size 13 (4) steel bars with specified yield of 413.7 MPa (60 ksi) with a cover of at least 3.8 cm (1.5 in.). Figure 3.2 shows a cross section of the Millville Bridge.



Figure 3.1 View of Millville Bridge

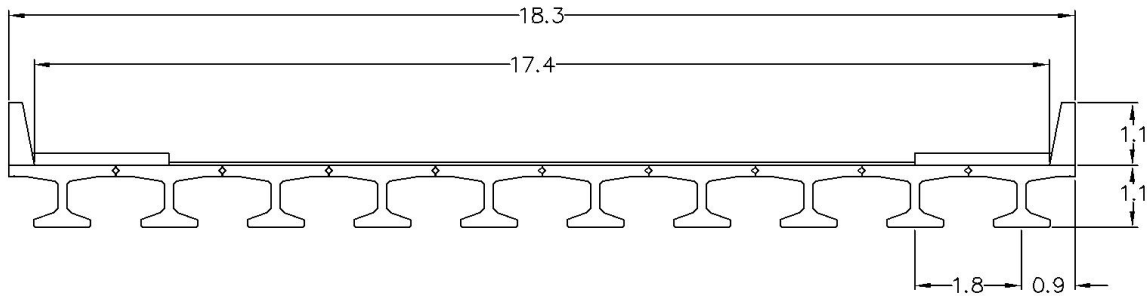


Figure 3.2 Bridge Cross-Section (dimensions given in meters)

The girders supporting the deck superstructure were cast using precast deck bulb tee sections. Each girder is 27.3 m (89.5 ft) long and 1.1 m (3.5 ft) tall. Girder dimensions are provided in Figure 3.4. The girders were prestressed prior to shipping to the job site using a harped strand profile. This harped strand profile includes 34 total strands, of which 24 are straight and 10 are harped strands. The harping points are located 10.9 m (35 ft 10 in.), which is $0.4L$, from the ends of the girder on either side. The centroid for all strands at mid-span are located at 9.52 cm (3-3/4 in.) from the bottom of the girders. At the girder ends, the centroid of the strands is located 0.9 m (3 ft) and 7.30 cm (2-7/8 in.) from the bottom of the girders for the harped and straight strands, respectively. Therefore, the composite strand centroid at the end of the girder is 320.5 mm (12.6 in.). Figure 3.3 shows a diagram of the harped strands for this bridge. The prestressing strands are 1.5 cm (0.6 in.) diameter, seven wire, low relaxation cables. The prestressing strands have a specified yield of 1862 MPa (270 ksi). The final jack prestressing force was 5.61 MN (1260.1 kips), equaling 1397 MPa (202.5 ksi). Figure 3.5 shows the girder in the casting bed at the prestress yard.

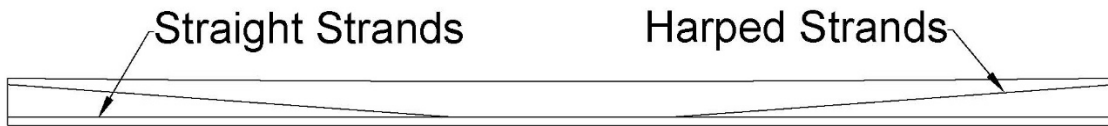


Figure 3.3 Harped Strands Diagram

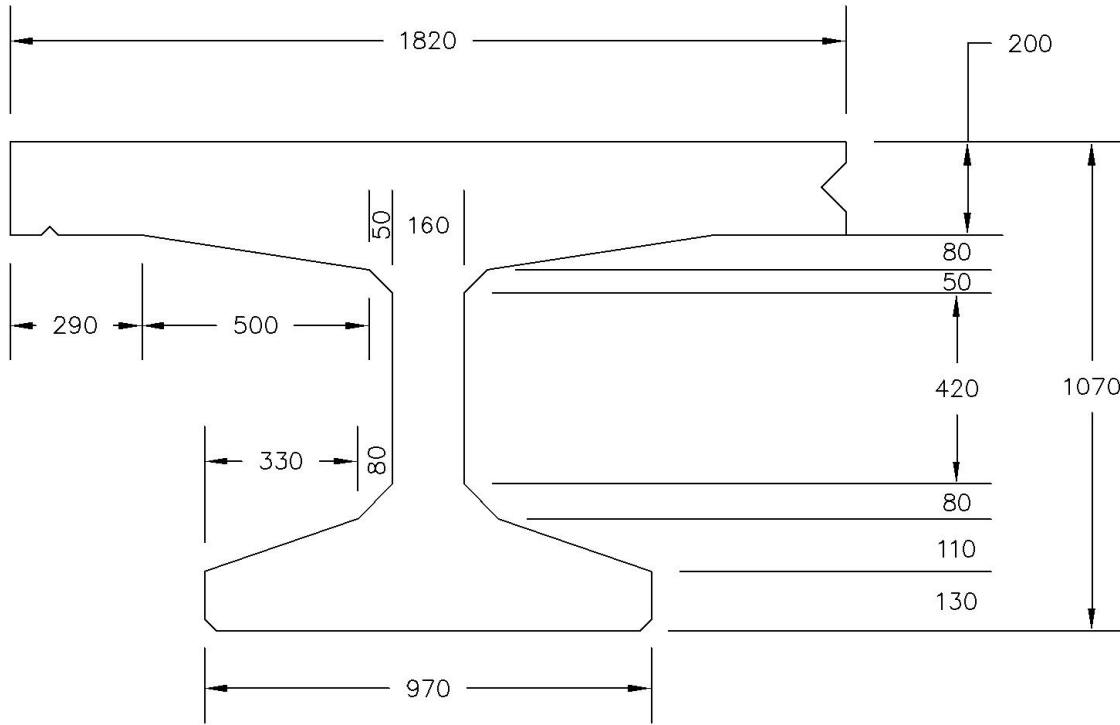


Figure 3.4 Girder Dimensions (dimensions are given in mm)



Figure 3.5 Girder in the Casting Bed at the Prestress Yard

As part of the bridge superstructure, there are two intermediate diaphragms located at the third points of the span. These diaphragms are made of MC 18 x 42.7 steel channels and connect to the webs of the adjacent girders. The exception is when the diaphragm accommodates a 50.8 cm (20 in.) steel casing between girders 3 and 4 that is placed longitudinally along the length of the bridge, in which case the diaphragm is composed of a 0.3 m (1 ft) thick reinforced concrete section. Figure 3.6 shows a picture of the diaphragm of the bridge.



Figure 3.6 Millville Bridge Diaphragm

The end supports of the Nibley Bridge superstructure were designed as fixed abutments using 0.7 m (2 ft. 3 in.) thick and 2.7 m (9 ft) tall concrete sections that are perpendicular across the width of the bridge. The abutments are designed to transfer the load from the girders to eight 0.3 m (12-3/4 in.) diameter concrete driven piles. Wing walls were cast adjacent to both abutment ends and are positioned parallel to the bridge with a total length of 3.7 m (12 ft), a width of 0.5 m (1.5 ft), and a height of 3.5 m (11.5 ft). Figure 3.7 shows a picture of the Millville Bridge abutments.



Figure 3.7 Millville Bridge Abutments

3.2 Instrumentation Plan

The Millville Bridge was instrumented with permanently embedded instrumentation designed to monitor long-term changes in strain and temperature. The overall plan was to embed sensors in two girders so instrumentation locations for each girder would exist at the mid-span and the end. These instrumentation locations would provide an approximate temperature profile over one-quarter of the bridge and changes in prestress for an interior and exterior girder. Symmetry could reasonably be applied to obtain a temperature profile of the entire bridge. Instrumentation Sites A and B are located on Girder 1 (G1); Site C, Site D, and Site E are located on Girder 5 (G5). Site A and Site C are located 0.23 m (9 in.) from the girder end. Site B and Site D are located at the mid-span (13.41 m [44 ft] from girder end). Site E is located 6.82 m (22 ft 5 in.) from girder end. Figure 3.8 shows a diagram of the locations of the instrumentation sites.

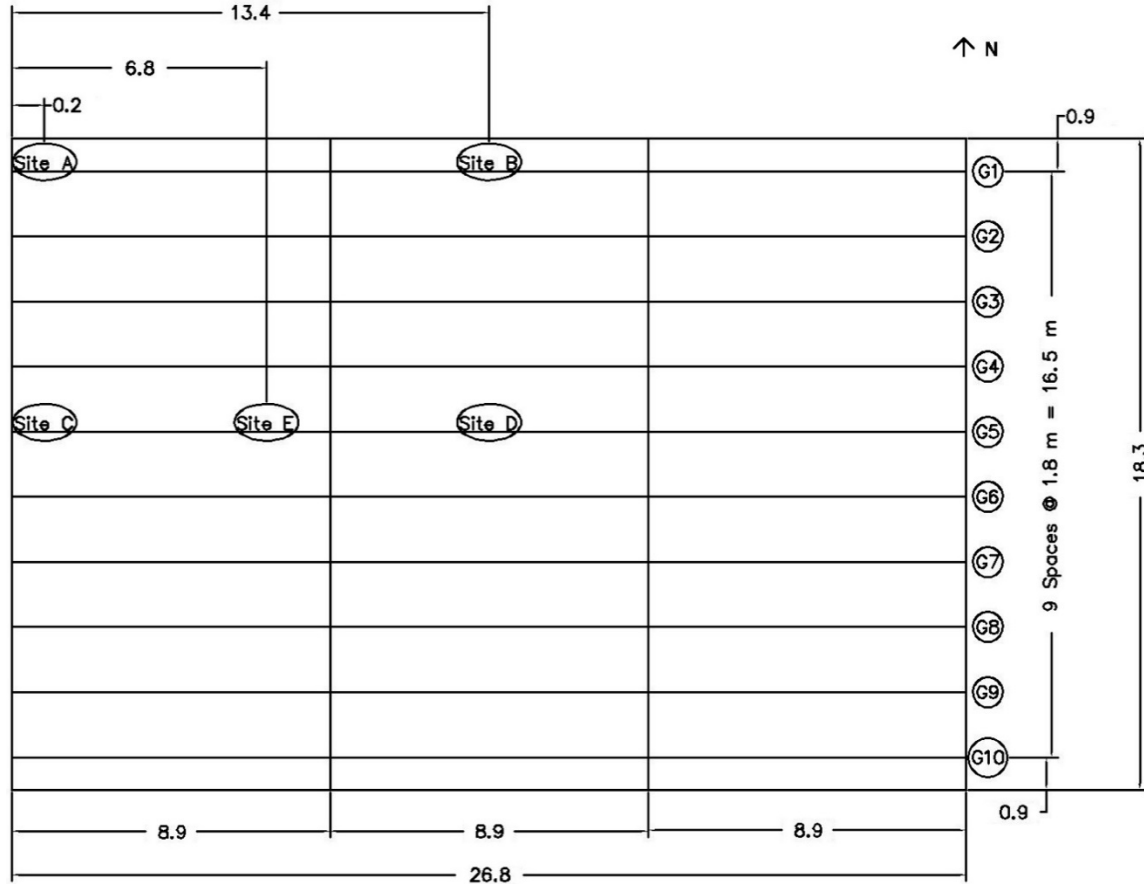


Figure 3.8 Instrumentation Site Layout Plan (dimensions in meters)

To measure the change in prestress and daily temperature variations for the bridge girders, the bridge was instrumented with a total of 16 Geokon model 4200 vibrating wire strain gauges with integral thermistors and 50 thermocouples. The strain gauges were embedded prior to casting at four bridge locations, shown as Site A, Site B, Site C, and Site D. Figure 3.9 shows a picture of the instrumentation installed in the casting yard at Site B. Sites A, C, and D were instrumented similarly. At each instrumentation cross section, two strain gauges were placed in the girder web (shown in Figure 3.10 as UW and LW) and the remaining two at the bottom of the girder (shown in Figure 3.10 as BL and BR). At Sites B and D, gauges BR and BL corresponded to the centroid of the prestressing steel. Due to the high congestion of steel at the end of the girder (Sites A and C), it was not physically possible to install gauges BR and BL at the centroid of the prestressing steel. Therefore, they were placed at the same elevation as BR and BL at Sites B and D. UW is located 61 cm (24 in.) from the bottom of the girder, and LW is located 44 cm (17-3/8 in.) from the bottom. BL and BR are located 10 cm (3-3/4 in.) from the bottom and 18 cm (7 in.) from the centerline.



Figure 3.9 Typical Instrumentation Site

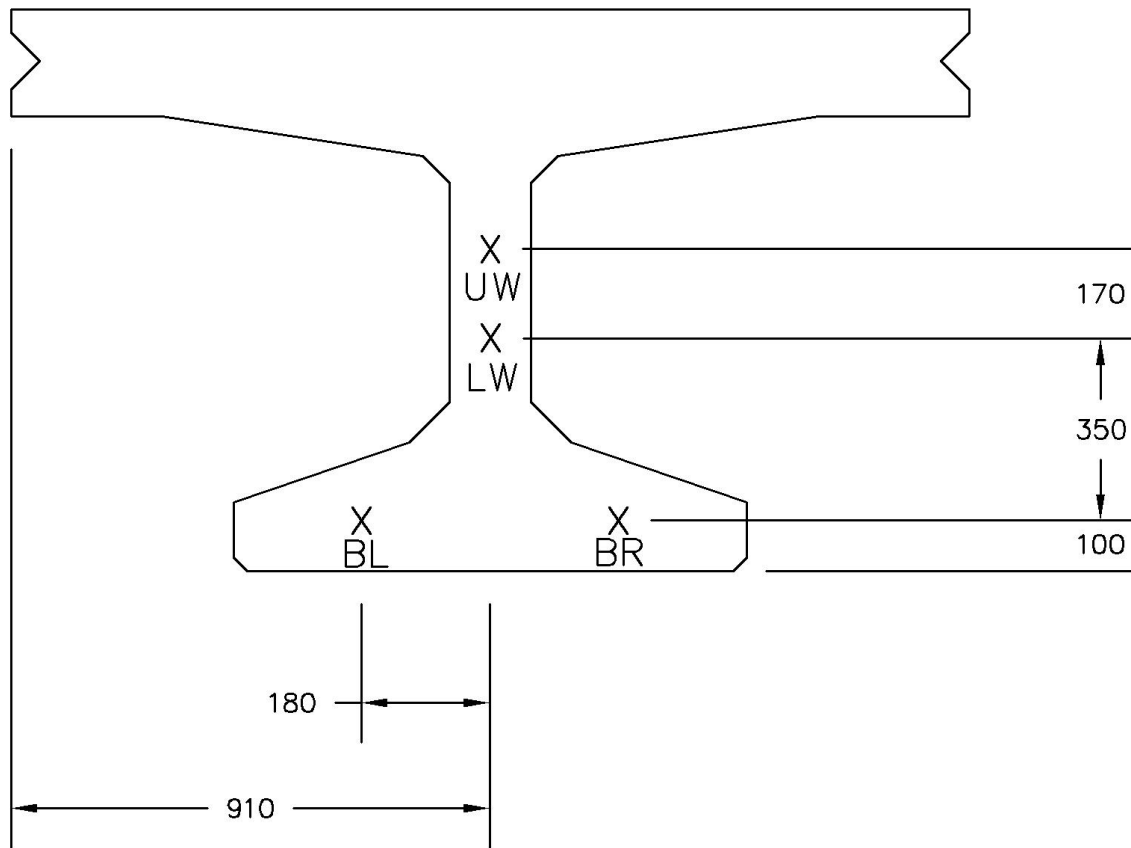


Figure 3.10 Typical Girder Instrumentation Plan (Dimensions in mm)

To measure the thermal gradient and mean temperature throughout the bridge superstructure, Type E thermocouples were embedded in groups of ten. The thermocouples were more densely placed toward the top of the deck, and the spacing gradually increased farther away from the top of the deck. Figure 3.11 shows the PVC pipe that was used to provide the spacing for each thermocouple group. These thermocouple groups were embedded at Site A, Site B, Site C, and Site D. The thermocouples are numbered 1 through 10, with 1 being closest to the deck surface and 10 being the farthest from the surface. At Site E, two thermocouple groups were embedded, one near the deck surface and another near the bottom of the girder. These groups consisted of five thermocouples. The groups of five thermocouples were spaced the same as the top five thermocouples at sites A through D. Thermocouples were prepared and covered with epoxy to provide a reliable and durable connection. For ease of placement during girder casting, holes were drilled in a 25.4 mm (1 in.) diameter PVC pipe, and thermocouples were placed such that 0.64 cm to 1.27 cm ($\frac{1}{4}$ in. to $\frac{1}{2}$ in.) of the thermocouple wire was showing on the exterior of the PVC. The tube was filled with an epoxy compound and epoxy glue was placed over the exposed thermocouple wires to protect against corrosion. The thermocouples were spaced in the thermocouple groups as follows: 0 cm, 0.64 cm, 1.27 cm, 1.91 cm, 3.18 cm, 4.45 cm, 6.99 cm, 9.52 cm, 13.34 cm, 17.15 cm (0 in., $\frac{1}{4}$ in., $\frac{1}{2}$ in., $\frac{3}{4}$ in., $1\frac{1}{4}$ in., $1\frac{3}{4}$ in., $2\frac{3}{4}$ in., $3\frac{3}{4}$ in., $5\frac{1}{4}$ in., and $6\frac{3}{4}$ in.). These thermocouple groups were embedded such that 5.08 cm (2 in.) of asphalt and 64 mm (0.25 in.) covered the top thermocouple.

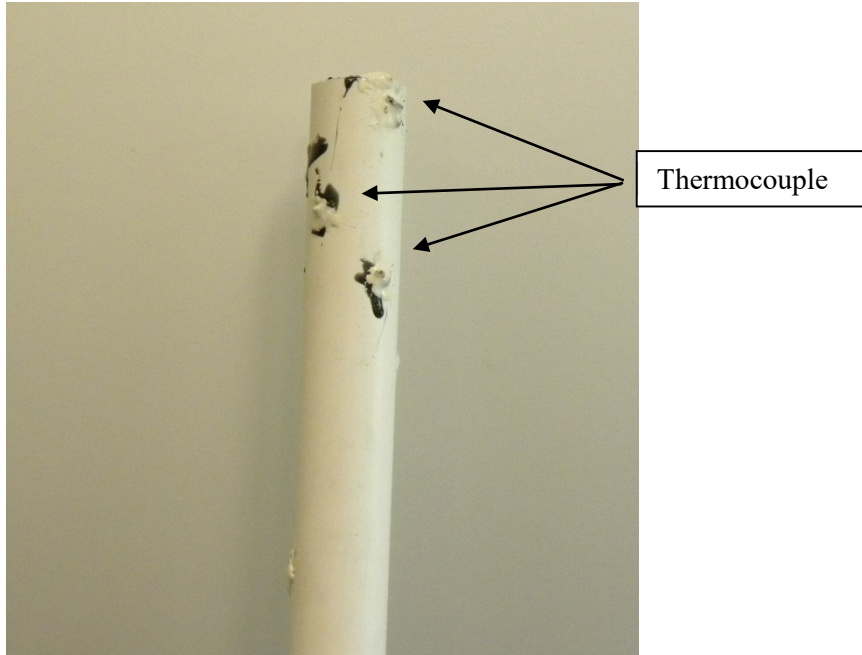


Figure 3.11 Typical Bank of Thermocouples

A Campbell Scientific CR3000 datalogger was initially used for Girder 5 to record changes in temperature. After casting, the CR3000 datalogger was switched to a CR1000 once the girders were delivered and placed at the bridge site. A CR1000 datalogger was used continuously for Girder 1. Measurements were taken every minute during curing and up to two weeks after girder placement, after which measurements were taken every 15 minutes.

The bridge girders were cast in December of 2015 and were shipped to the bridge site during January 2016. Work continued on the bridge from January through May, when the bridge was completed.

3.3 Prestress Loss Data

Measured changes in strain were used to calculate the prestressing losses in the prestressing strands. The strain measurements for this portion of the study began immediately prior to the release of the prestressing cables and ended February 29, 2016. The prestressing cables for Girder 5 were released on December 8, 2015, and changes in strain were measured for approximately 2,010 hours (83.75 days). The prestressing cables for Girder 1 were released on December 14, 2015, and changes in strain were measured for approximately 1,861 hours (77.54 days). The change in strain study has two principal time periods: (1) strain losses during initial destressing to determine the elastic shortening losses, and (2) long-term strain losses.

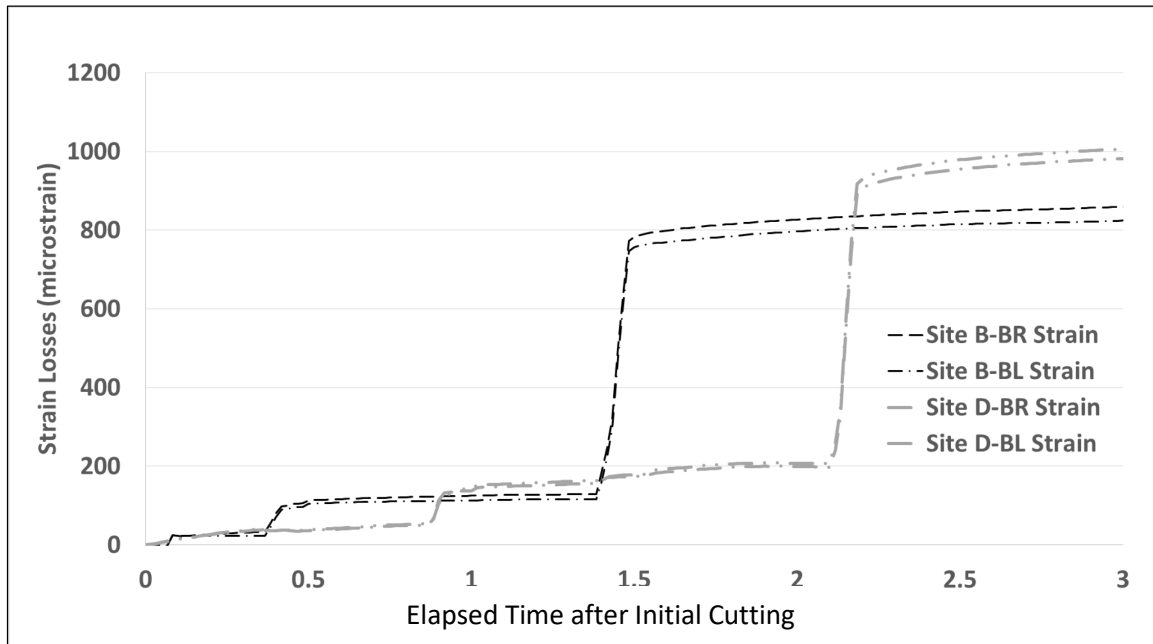
Table 3.1 lists the comparative tested concrete strengths over time and the design strengths. It is important to note that Girder 5 was released after one day of curing; whereas, Girder 1 was released after curing over a weekend. Both girders were cured under similar circumstances. Steam was applied to Girder 1 over the weekend only to maintain a minimum temperature of 10°C (50°F). The steam curing was increased on Monday prior to release of the strands.

Table 3.1 Comparative Concrete Strengths

Girder	Date Poured	Date Released	Design Release Strength MPa (psi)	Design Ultimate Strength MPa (psi)	Release Strength MPa (psi)	7-Day Strength MPa (psi)	28-Day Strength MPa (psi)
5	12/7/2015	12/8/2015	41.37 (6,000)	58.61 (8,500)	46.33 (6,720)	63.98 (9,280)	81.15 (11,770)
1	12/9/2015	12/14/2015	41.37 (6,000)	58.61 (8,500)	47.64 (6,910)	60.88 (8,830)	75.45 (10,943)

3.3.1 Strain Losses during Initial Destressing

Figure 3.12 shows a comparison of the initial prestress losses at the centroid of the prestressing cables during destressing of the cables at the mid-span of girders 1 and 5. The prestress losses were calculated by multiplying the measured strain by the modulus of elasticity of the cable (Equation 3.1). Table 3.2 lists the average prestress losses due to elastic shortening at mid-span for girders 1 and 5. Time zero for all prestress loss figures was taken on December 14, 2015, at 10:36 AM and December 8, 2016, at 5:23 AM for Girder 1 and Girder 5, respectively.

**Figure 3.12** Strain Losses during Bridge Initial Destressing

The jumps in strain measurements are due to cutting of a portion of the prestressing strands. During destressing, the harped strands were cut first. The smaller changes in strain before 1.5 hours and 2.0 hours for Sites B and D are due to the harped strand cuts. Figure 3.12 shows the effect of the initial strand cutting of the harped strands, followed by the large change in strain due to the cutting of the straight strands. The elastic shortening losses were taken as the difference in strain immediately prior to the cutting of the strands until the cutting of the last prestressing strand. Site D (Girder 5) took longer to destress in comparison with Site B (Girder 1). As a result, creep was observed to occur, especially between the 1- and 2-hour marks. This creep was subtracted out of the elastic shortening losses. After the

elastic shortening losses had occurred, the long-term prestressing losses of creep and shrinkage could be identified.

$$\sigma = E\varepsilon \quad \text{Equation 3.1}$$

Where: σ =stress loss in prestressing strands; E =modulus of elasticity of the prestressing strands, taken as 196.5 GPa (28,500 ksi); ε =strain loss measured by strain gauges.

As shown in Table 3.2, the elastic shortening loss was approximately 18.8 MPa (2.73 ksi) lower for Girder 1 than Girder 5. While the curing times were different for each girder, the release strength was longer for Girder 5 and is believed to be the cause of the higher elastic shortening losses.

Table 3.2 Elastic Shortening Loss Comparison at Mid-span for Girder 1 and Girder 5

Girder	Elastic Shortening Losses ($\mu\varepsilon$)	Elastic Shortening Losses (MPa)	Elastic Shortening Losses (ksi)
1	759.8	149.3	21.65
5	855.3	168.1	24.38

Once the girder strands were cut, they were lifted from the bed and transported to a field where they continued to cure and finish work was performed. When the girders were lifted from the casting bed, a change in strain was observed at all strain gauge sites. This change in strain is believed to be a combination of restraint moment developed in the casting bed due to friction and change in boundary condition. The moment induced by friction in the casting bed caused a decrease in the strain losses that otherwise would have occurred. Figure 3.13 shows the increase in recorded strain as the girder was lifted out of the casting bed and during transporting of the girder in the casting yard at sites B-BR, B-BL, D-BR, and D-BL. Linear regression lines were calculated from the data from before the girder was removed from the bed and after the girder was placed in the yard. The strains after the girder was placed in the yard were compared with the linear regression line from when the girder was in the bed. Also, the strains from before the girder was removed from the bed were compared with the linear regression lines of the strains from when after the girder was placed in the yard. Figure 3.14 shows an example of the linear regression lines used to calculate the friction loss reductions. The average values of the friction loss reductions are presented in Table 3.3.

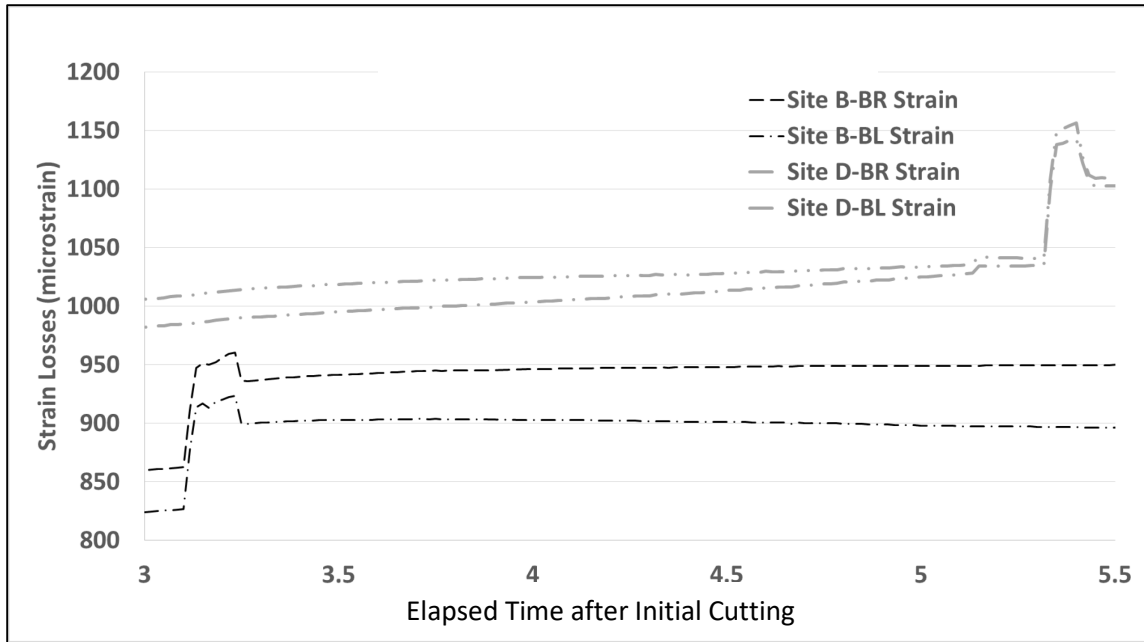


Figure 3.13 Increases in Strain Losses Due to Transporting Girder from Bed to Yard

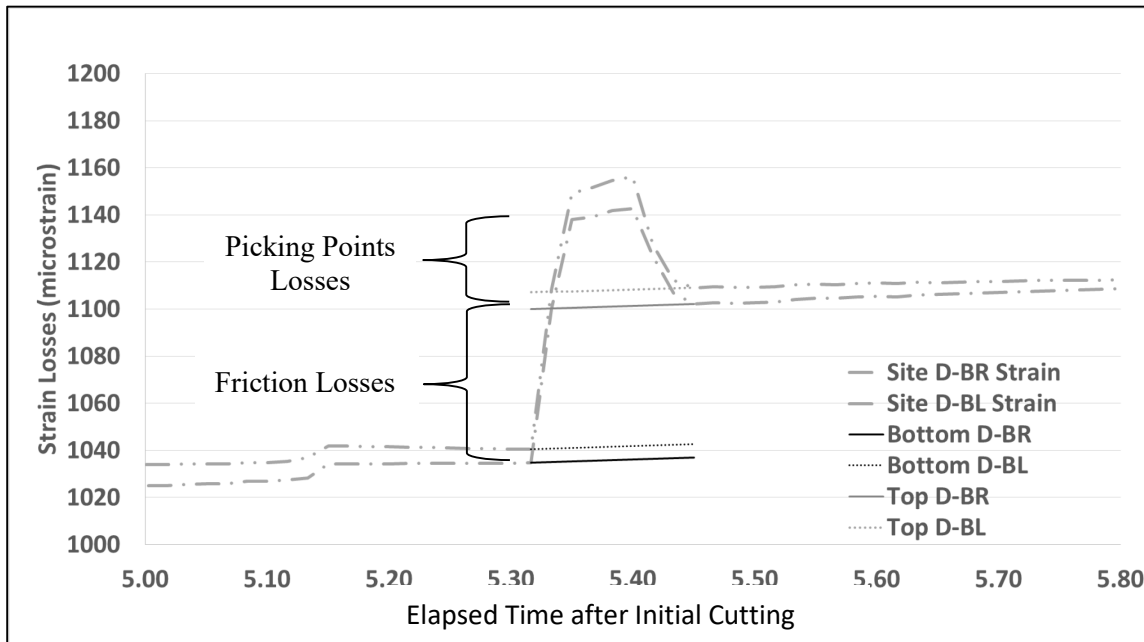


Figure 3.14 Linear Regression Example Used for Friction and Picking Points Loss Calculations

Table 3.3 Loss Reductions Due to Friction in Casting Bed

Site	Strain Loss Reduction Due to Friction (mε)	Stress Loss Reduction Due to Friction (MPa)	Stress Loss Reduction Due to Friction (ksi)
B-BR	70.2	13.79	2.00
B-BL	70.0	13.79	2.00
D-BR	65.2	12.81	1.86
D-BL	66.5	13.07	1.90

The friction force required to produce this reduction in prestress losses was calculated using the following equation:

$$F_f = \frac{I_g E_{ps} \varepsilon_f}{e_f y_{ps}} \quad \text{Equation 3.2}$$

Where: F_f = force of friction; I_g = gross moment of inertia; E_{ps} = modulus of elasticity of the prestressing steel; ε_f = measured friction strain loss reduction; e_f = eccentricity of the friction, taken as the distance from the centroid of the section to the bottom of the girder; y_{ps} = distance from the centroid of the section to the centroid of the prestressing strands. I_g was taken as 10,365,450 cm⁴ (249,031 in.⁴), e_f was taken as 65.5 cm (25.8 in.), y_{ps} was taken as 56 cm (22.0 in.), and E_{ps} was taken as 196.5 GPa (28,500 ksi). Using the strains in Table 3.3 and Equation 3.2, the calculated friction forces are presented in Table 3.4.

Table 3.4 Calculated Friction Force in Casting Bed

Site	Friction Force (MN)	Friction Force (kips)
B-BR	3.897	876.0
B-BL	3.886	873.5
D-BR	3.619	813.6
D-BL	3.691	829.9

All losses greater than losses from releasing the girder from the casting bed are due to picking up the girder at the lifting loops and creep during transport in the casting yard. The lifting loops are 2.13 m (7 ft.) from the edge of the girder, causing the self-weight moment to decrease. These picking point losses are the initial losses greater than the top linear regression lines in Figure 3.14. The picking point losses at the centroid of the prestressing strands at mid-span are reported in Table 3.5.

Table 3.5 Strain Losses Due to Yard Girder Picking Points

Site	Picking Points Strain Loss (με)	Picking Points Stress Loss (MPa)	Picking Points Stress Loss (ksi)
B-BR	12.85	2.53	0.37
B-BL	15.34	3.01	0.44
D-BR	37.4	7.35	1.07
D-BL	41.7	8.18	1.19

The measured results were compared with the predicted results using the following equation:

$$\varepsilon = \frac{\Delta M_{sw} y_{ps}}{I_g E_p} \quad \text{Equation 3.3}$$

Where: ε = predicted picking points loss; ΔM_{sw} = change in self-weight moment from lifting the girder with lifting loops to the simply supported condition; y_{ps} = distance from section centroid to the centroid of the prestressing steel; I_g = section gross moment of inertia; E_p = modulus of elasticity of the prestressing steel. The following equation was used to calculate the change in self-weight moment:

$$\Delta M_{sw} = \frac{wl^2}{8} - \frac{lw}{2} \left(\frac{l}{4} - l_1 \right) \quad \text{Equation 3.4}$$

Where: w = self-weight intensity; l = full length of girder; l_1 = length from the end of the girder to the lifting loop. Using the concrete unit weights provided by the casting yard and Equation 3.4, the predicted picking point losses were 12.4 $\mu\varepsilon$ and 12.5 $\mu\varepsilon$ for girders 1 and 5, respectively. Comparing these values with the measured values in Table 3.5 shows that the predicted value was within 12.0% of the average measured value for Girder 1. However, the predicted picking point loss for Girder 5 was 68.4% away from the average measured value.

Presented in Figure 3.15 and Figure 3.16 are the initial girder destressing strain losses for Girder 1. The initial girder destressing strain losses for Girder 5 are presented in Appendix A.

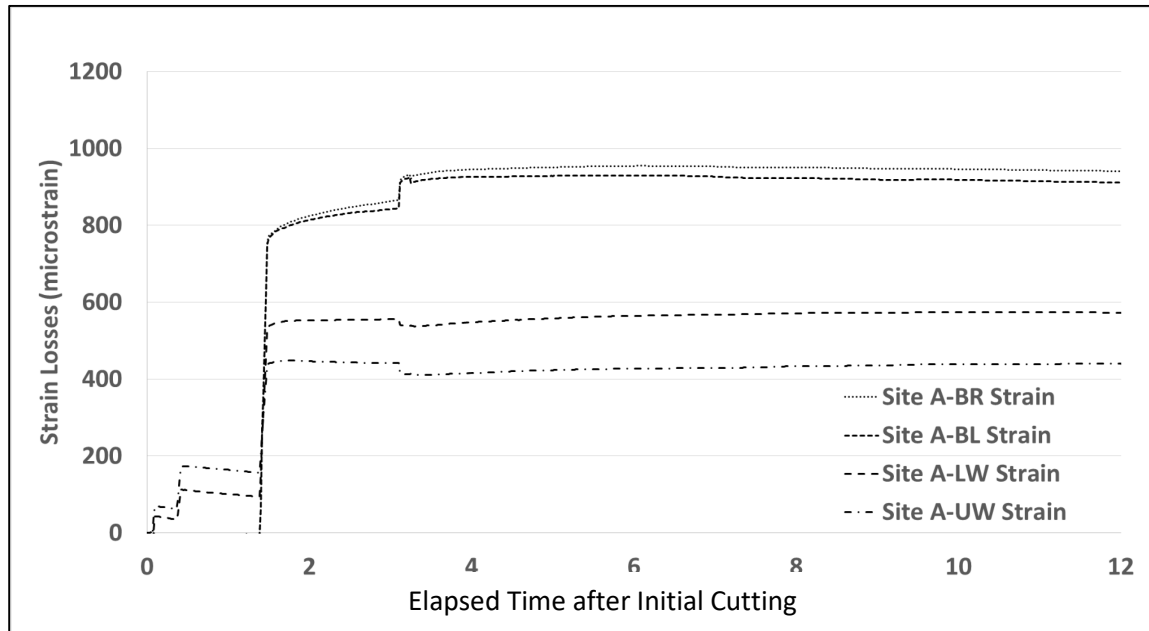


Figure 3.15 Initial Girder Destressing Strain Losses for Site A

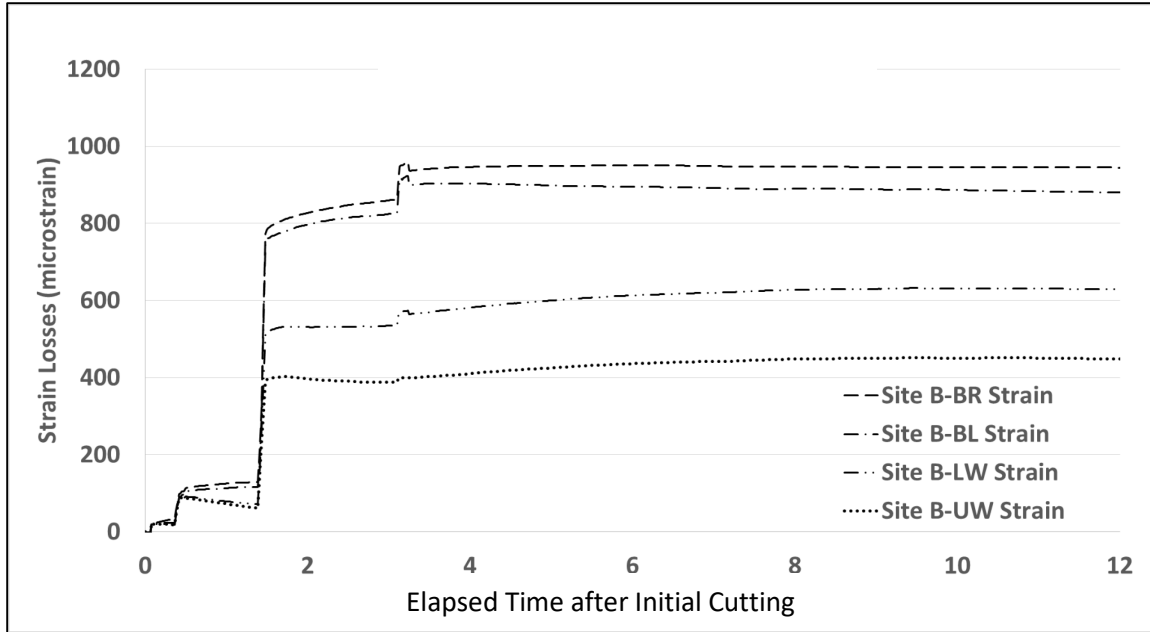


Figure 3.16 Initial Girder Destressing Strain Losses for Site B

As seen from Figure 3.15, Figure 3.16, Figure A.1, and Figure A.2, the strain losses were always higher at the end of the bridge. This is due to the lower self-weight moment at those locations and therefore higher compressive forces.

3.3.2 Long-Term Strain Losses

Strain data were recorded every minute from December 8, 2015, until January 27, 2016, and recorded at 15-minute averages after January 27. Data from December 21, 2015, at 11:23 a.m. through December 23, 2015, at 9:38 p.m. were not recorded due to the transportation of the girders to the bridge site. Figure 3.17 through Figure 3.19 show the strain losses measured at mid-span for girders 1 and 5 for the duration of this study.

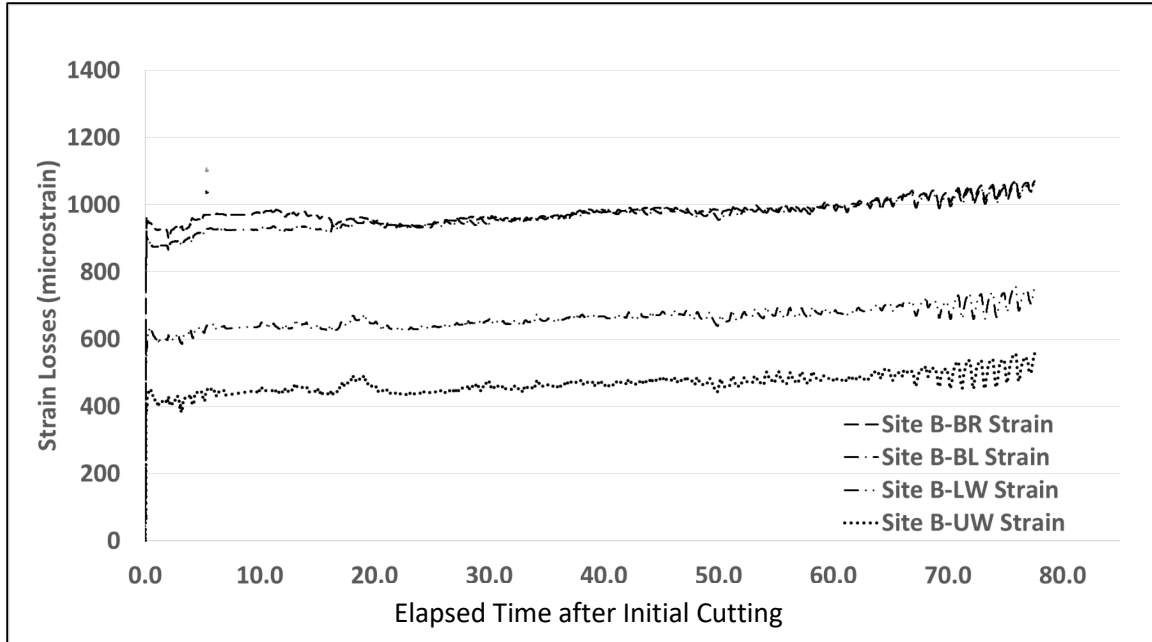


Figure 3.17 Long-Term Prestressing Steel Strain Losses at Mid-Span for Girder 1

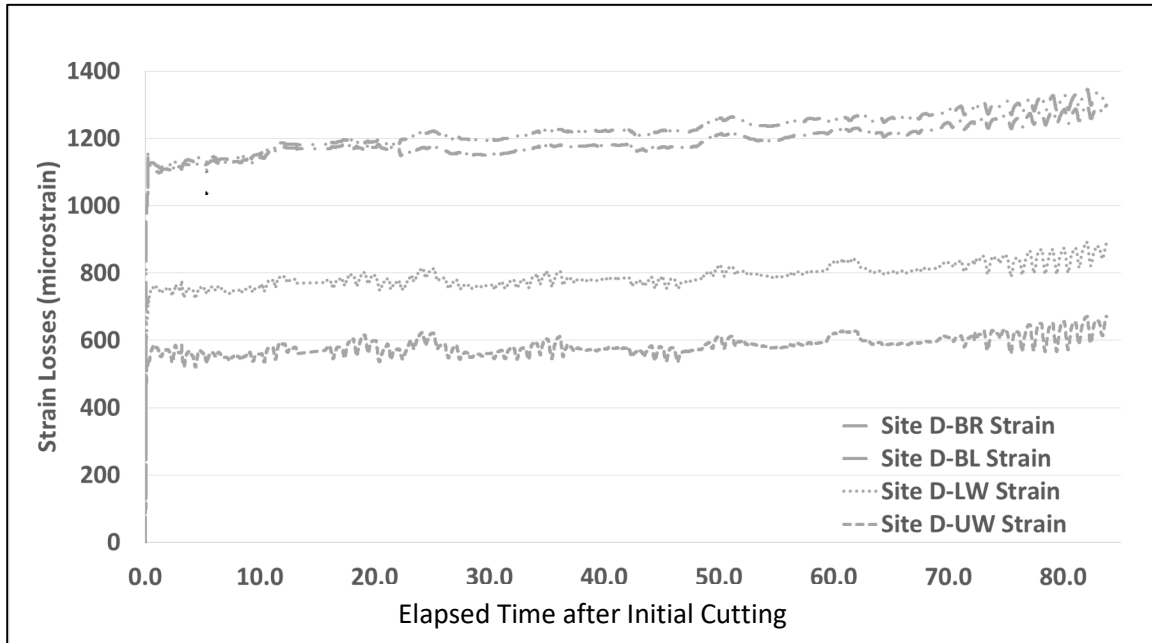


Figure 3.18 Long-Term Prestressing Steel Strain Losses at Mid-Span for Girder 5

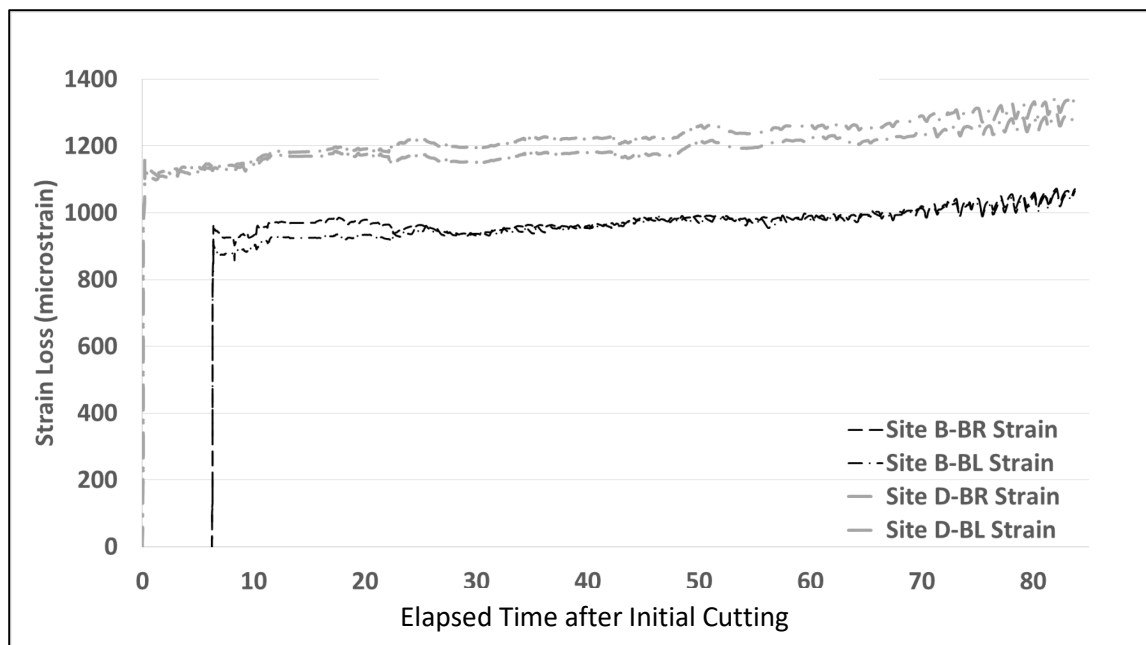


Figure 3.19 Long-Term Prestressing Steel Strain Losses at Mid-Span for Girders 1 and 5

As shown in Figure 3.17 through Figure 3.19, the long-term strain losses measured in this study follow an approximate linear increase after the initial losses have occurred. Girder 1 experienced an overall average 220.3 $\mu\epsilon$ larger strain loss than Girder 5. The maximum and minimum differences were 262.4 $\mu\epsilon$ and 128 $\mu\epsilon$, respectively. This difference occurred with the short-term losses, as the long-term rate of loss for both girders is approximately the same.

3.4 Temperature Data

3.4.1 Curing Temperature Data

Temperature data were measured at one minute intervals through the curing process for Girder 1. Girder 1 was cured over the weekend. All data recorded during this time are presented in Figure 3.20. This figure is primarily used to present the range of temperatures experienced by the girder, as individual thermocouple lines are not easily distinguishable. Time zero was taken as Wednesday, December 9, 2015, at 12:00 a.m. and temperatures are shown until Tuesday, December 15, at 12:00 a.m. As stated previously, steam was used as required to maintain the girder at the minimal programmed curing temperature over the weekend. Although the exact time is not known, the girder was most likely poured within the first nine hours on the figure. The highest temperature reached in curing was 66.59°C (151.86°F) and occurred at thermocouple B-10 on December 10, 2015, at 5:23 a.m. (29.4 hours in Figure 3.20). The lowest temperature experienced in curing was 8.51°C (47.32°F) and occurred at thermocouple B-1 on December 10, 2015, at 9:57 p.m. (46 hours in Figure 3.20). The cover over the girder was removed at approximately time 129 hours.

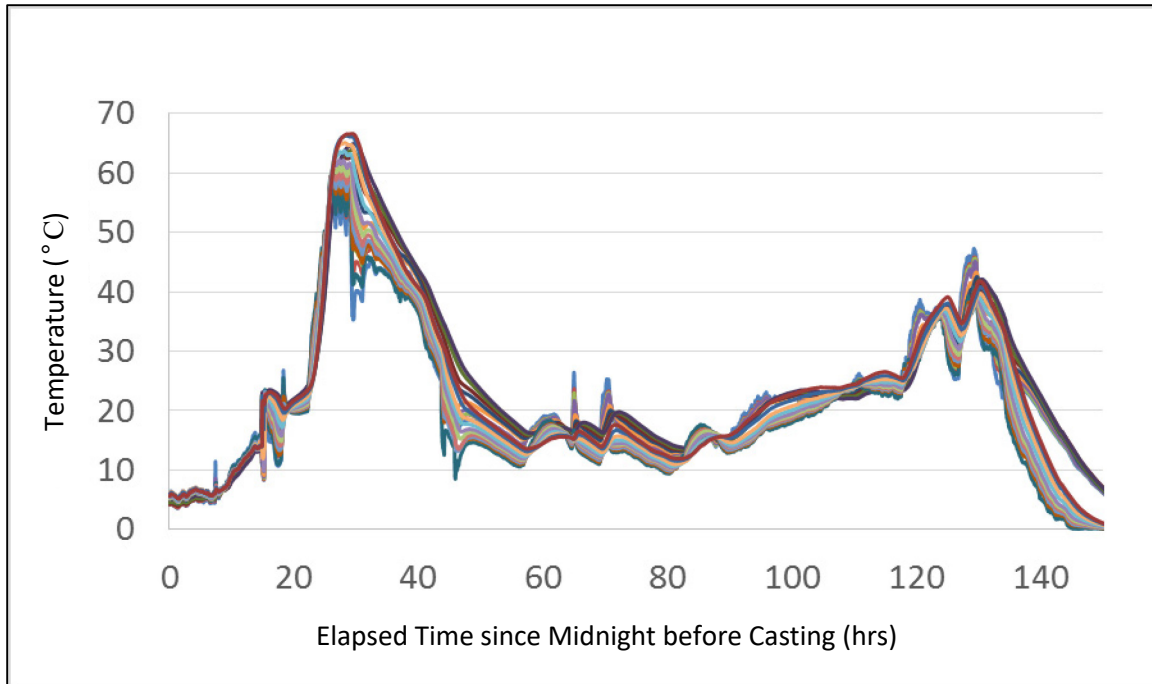


Figure 3.20 Girder 1 Temperatures during Curing

3.4.2 Temperature Gradients during Curing

Temperature gradients during curing were analyzed in two ways. The first was analyzed by taking the maximum difference between thermocouples 1 and 10. The minimum gradient was obtained similarly. The worst cases for the maximum and minimum cases are presented in Figure 3.21 and Figure 3.22. These figures present the depth versus temperature curve with zero depth equating to the top of the deck. The worst case temperature gradients information is presented in Table 3.6.

Table 3.6 Worst Case Temperature Gradients Information

Analysis	Site	Date	Time	Value Of Difference (°C)
Max. 1-10 Difference	A	12/10/2015	12:30 am	11.33
Min. 1-10 Difference	A	12/10/2015	5:32 am	-29.57

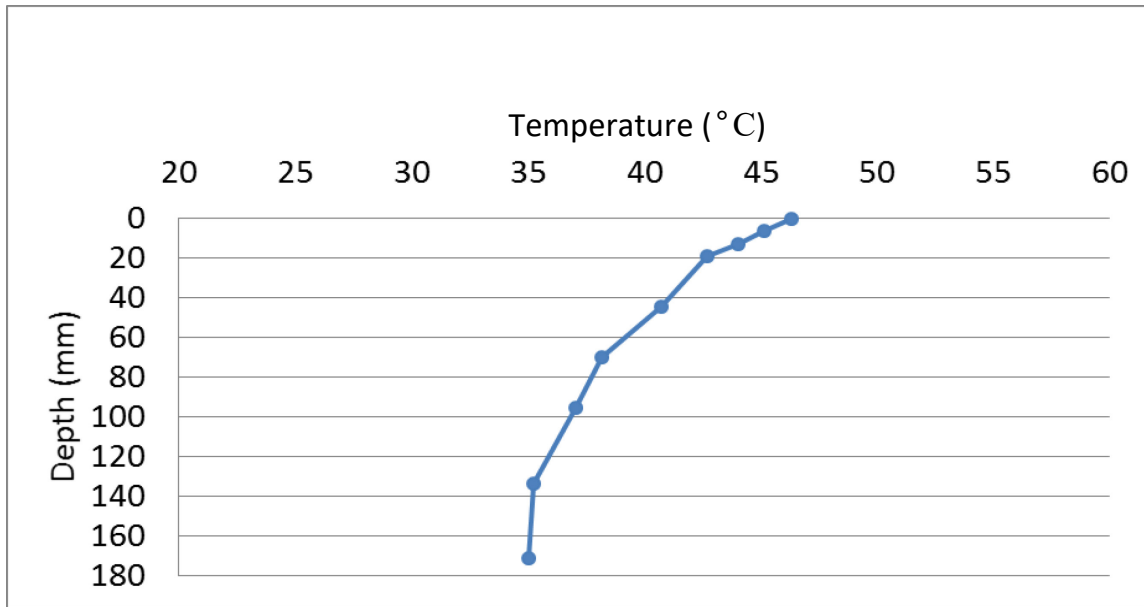


Figure 3.21 Maximum Temperature Gradient during Curing Using the Difference between Thermocouples 1 and 10

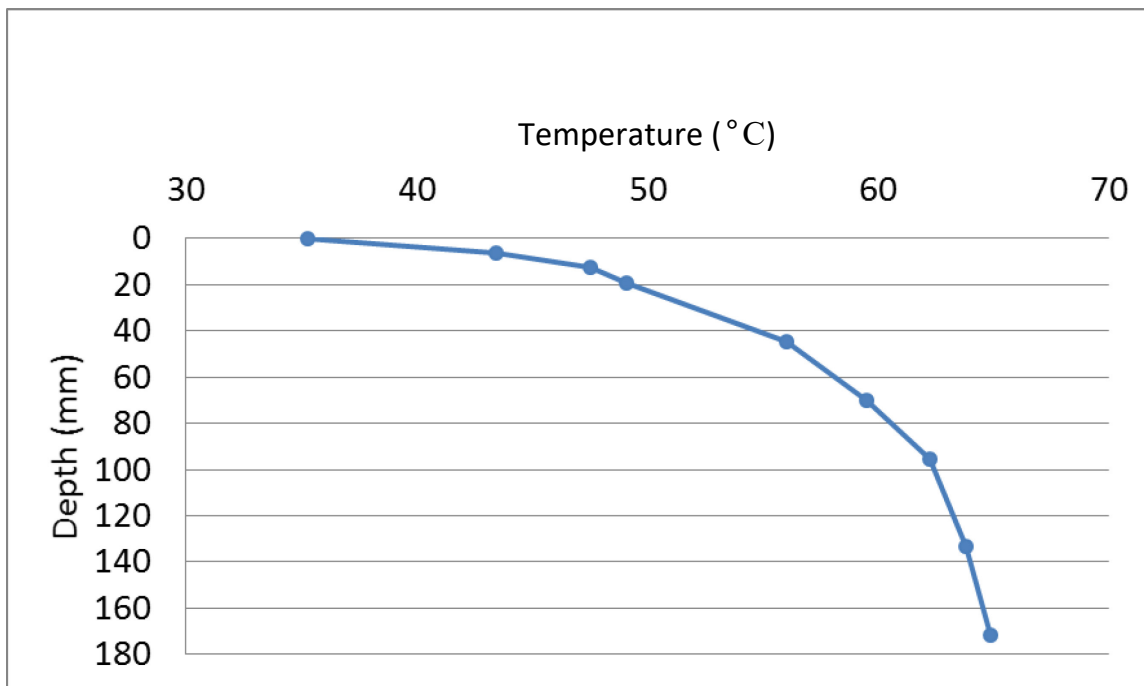


Figure 3.22 Minimum Temperature Gradient during Curing Using the Difference between Thermocouples 1 and 10

3.4.3 Long-Term Temperature Data

Temperature data for Girder 1 were recorded at one-minute intervals for the first 1,196 hours (49.8 days) and at 15-minute intervals after that. The data presented for Girder 1 in this section exclude the first 150 hours of data that were used to analyze the temperatures during the curing period. Temperature data for Girder 5 were recorded at 15-minute intervals throughout the length of this study. Time zero for all

temperature data began December 9, 2015, at 12:00 a.m. and December 8, 2015, at 5:45 a.m. for Girder 1 and Girder 5, respectively. Time zero in Figure 3.24 is after the cover was taken off the girder and less than an hour before the initial distressing. All recorded long-term temperature data are presented in Figure 3.23 and Figure 3.25 for girders 1 and 5, respectively. The VWSG temperature data for mid-span are presented in Figure 3.24 and Figure 3.26 for girders 1 and 5, respectively.

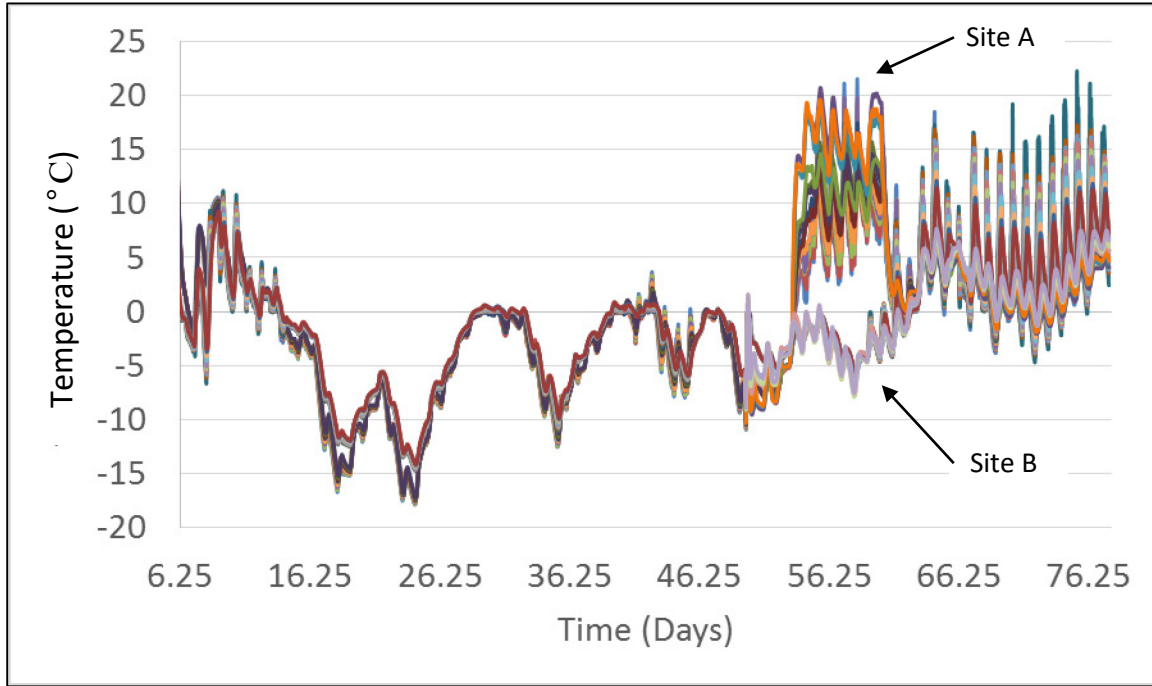


Figure 3.23 Girder 1 Long-Term Temperatures

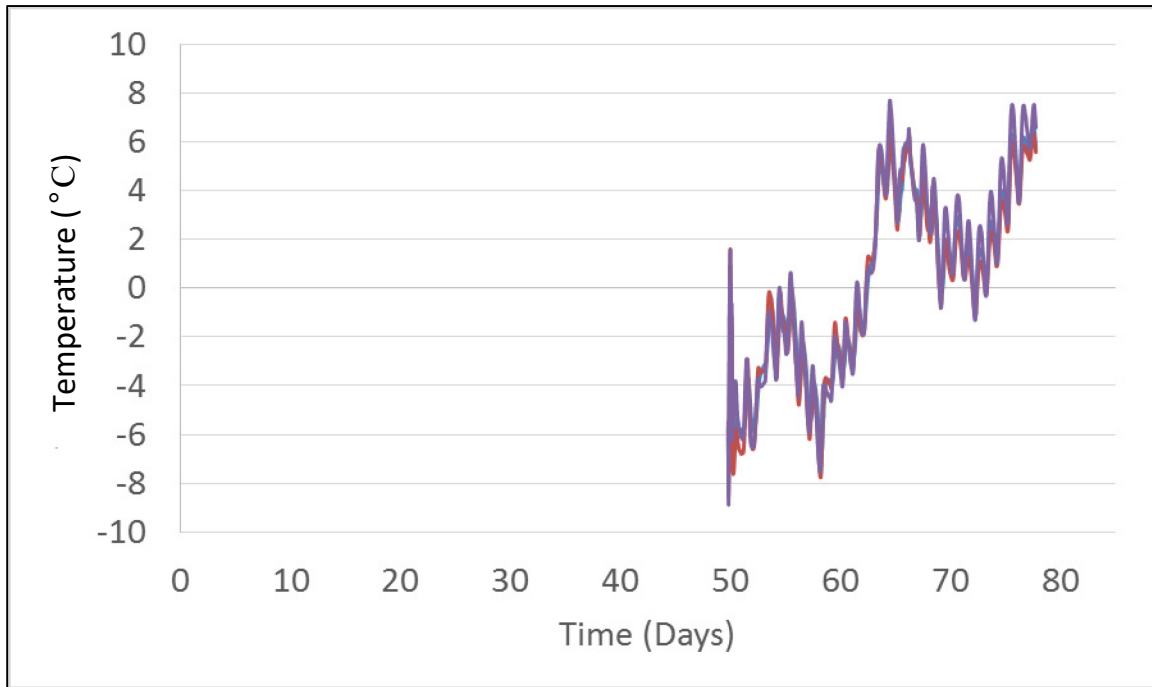


Figure 3.24 Girder 1 VWSG Temperatures at Mid-Span

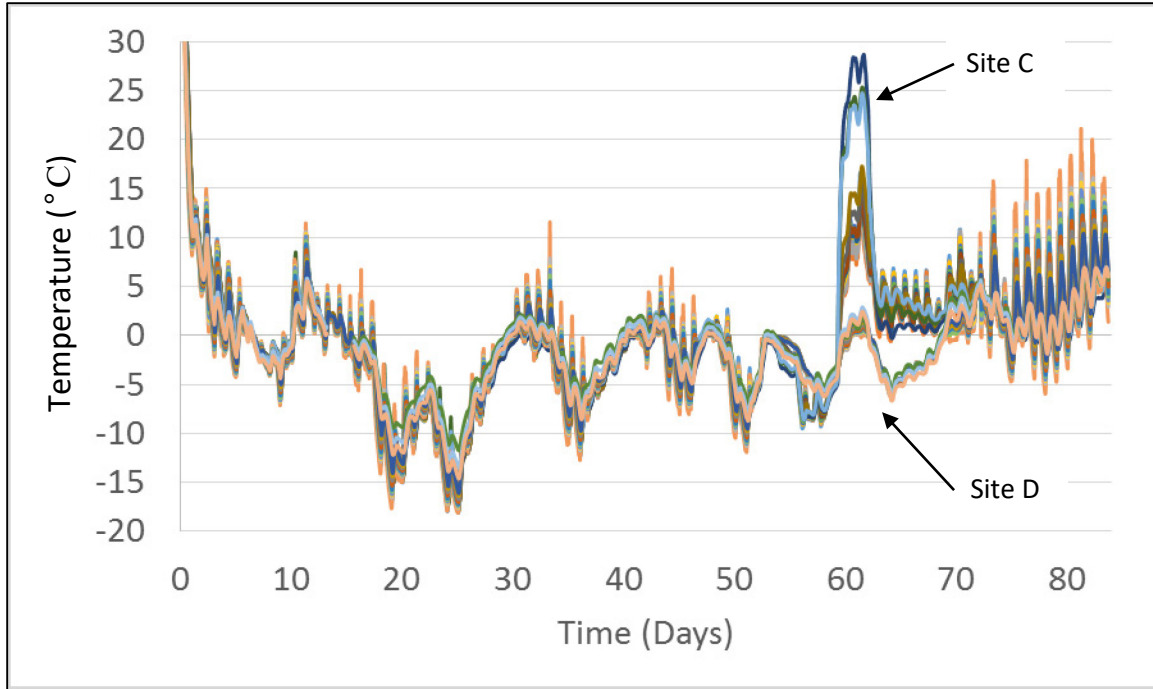


Figure 3.25 Girder 5 Long-Term Temperatures

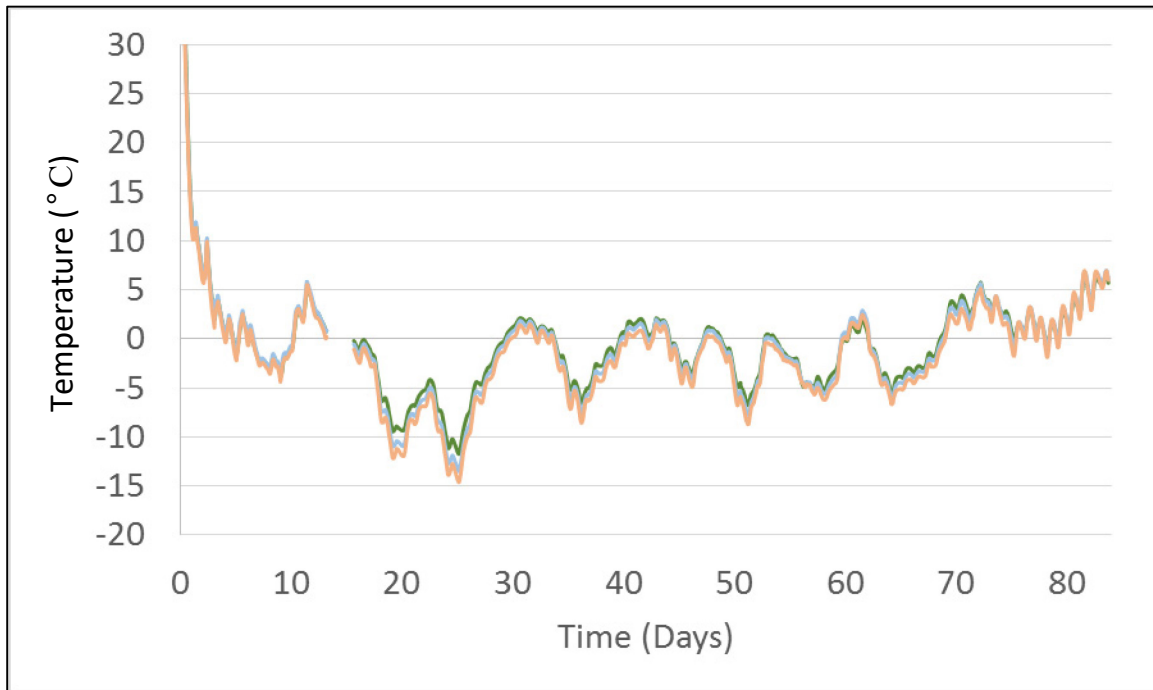


Figure 3.26 Girder 5 VWSG Temperatures at Mid-Span

As shown in Figure 3.23 and Figure 3.25, all of the data (end-span and mid-span) follow the same trends in data ranges. The exception is the data at about 56 and 60 days for Girder 1 and Girder 5, respectively. The sites with higher measured temperatures at these times are at the end-spans and are a result of the casting of the concrete bridge abutments. Temperature data after the casting of the abutments are presented in Figure 3.27 and Figure 3.28. The lower temperatures represent the temperatures at mid-span.

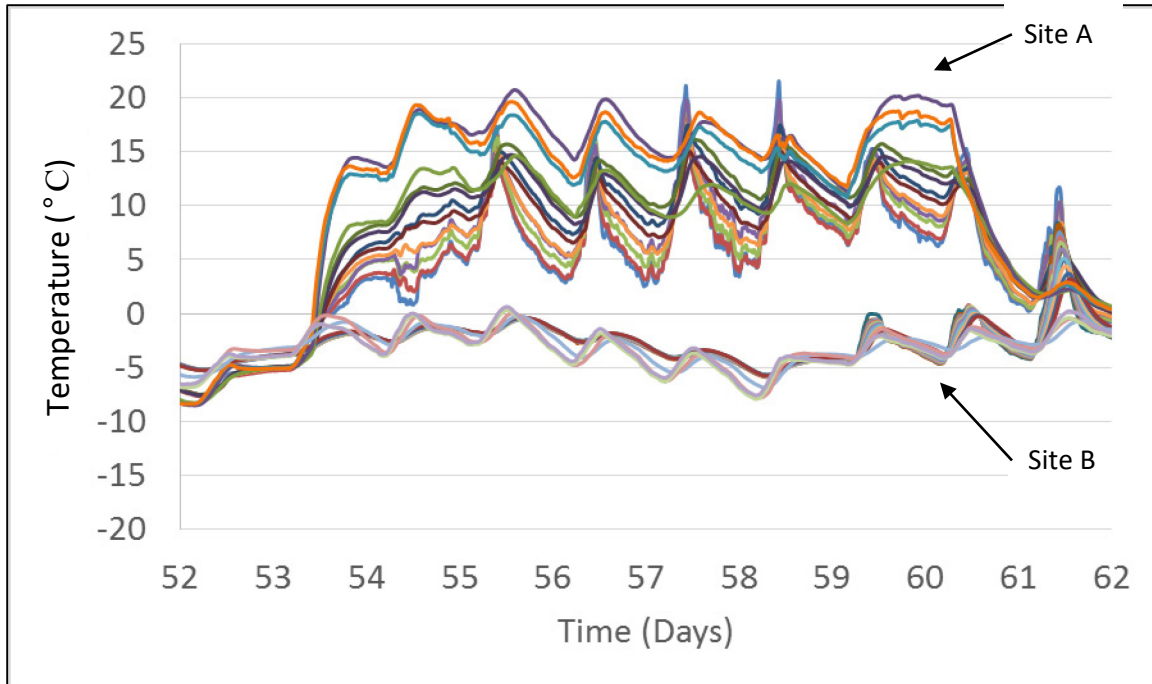


Figure 3.27 Girder 1 Temperatures during Abutment Casting

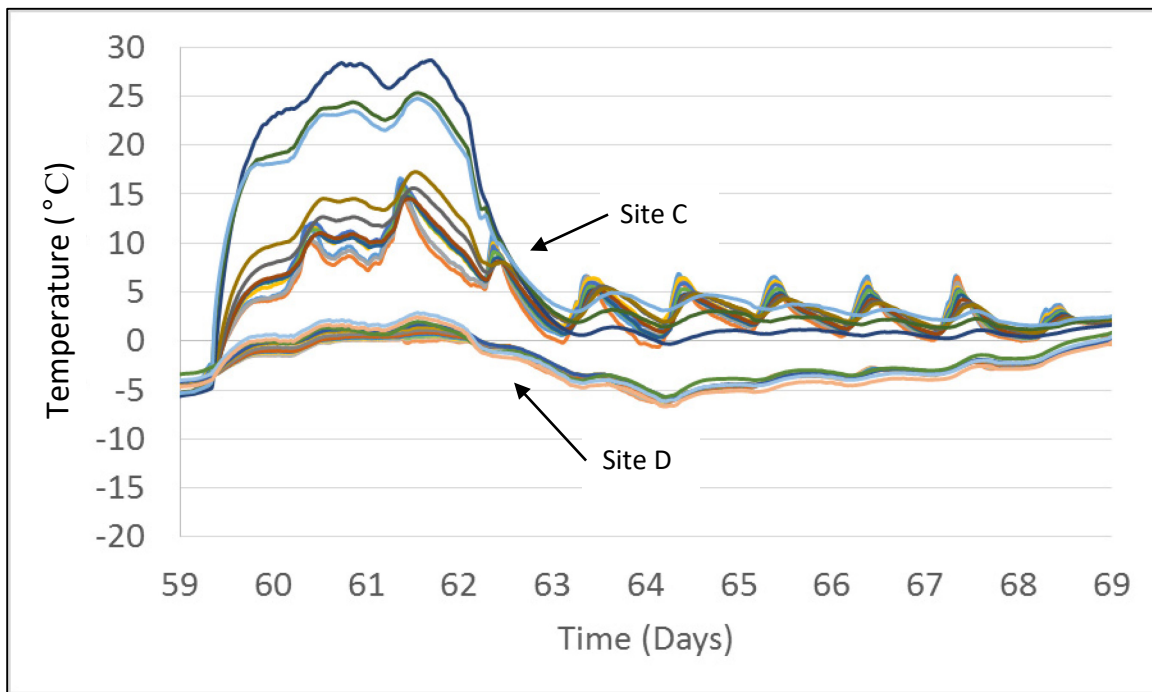


Figure 3.28 Girder 5 Temperatures during Abutment Casting

Based on the data from Figure 3.27 and Figure 3.28, Girder 1 showed a lower temperature difference between end-span and mid-span. However, this difference was spread over approximately seven days. Girder 5 showed a larger temperature difference; however, this lowered significantly after approximately three days and then had small temperature differences for the following six days.

3.4.4 Long-Term Temperature Gradients

Temperature gradients in this section were analyzed similarly to how they were analyzed during curing; i.e., they were analyzed two different ways:

- Maximum gradients using the difference between thermocouple 1 and VWSG UW
- Minimum gradients using the difference between thermocouple 1 and VWSG UW

The maximum temperature gradient is presented in Figure 3.29 for sites A, B, C, and D. This figure presents the depth vs. temperature curve with zero depth equating to the top of the deck. The greatest minimum temperature gradient experienced by the girders happened soon after the cover used in curing was removed. This temperature gradient was compared against the minimum temperature gradient experienced in the field. These temperature gradients are presented in Figure 3.30 and 3.31. This temperature differential information is presented in Table 3.7.

In addition to the temperature gradients at sites A, B, C, and D, gradients were analyzed at Site E, which shows temperatures throughout the girder section. Site E was analyzed separately from sites A, B, C, and D, and is presented in Section 3.4.5.

Table 3.7 Worst Case Temperature Gradients Information

Analysis	Site	Date	Time	Value of Difference (°C)
Max. 1-UW Difference	B	2/27/2016	12:45 pm	18.85
Min. Cooling 1-UW Difference	D	12/8/2015	6:15 am	-18.80
Min. Field 1-UW Difference	D	12/10/2015	8:00 pm	-6.63

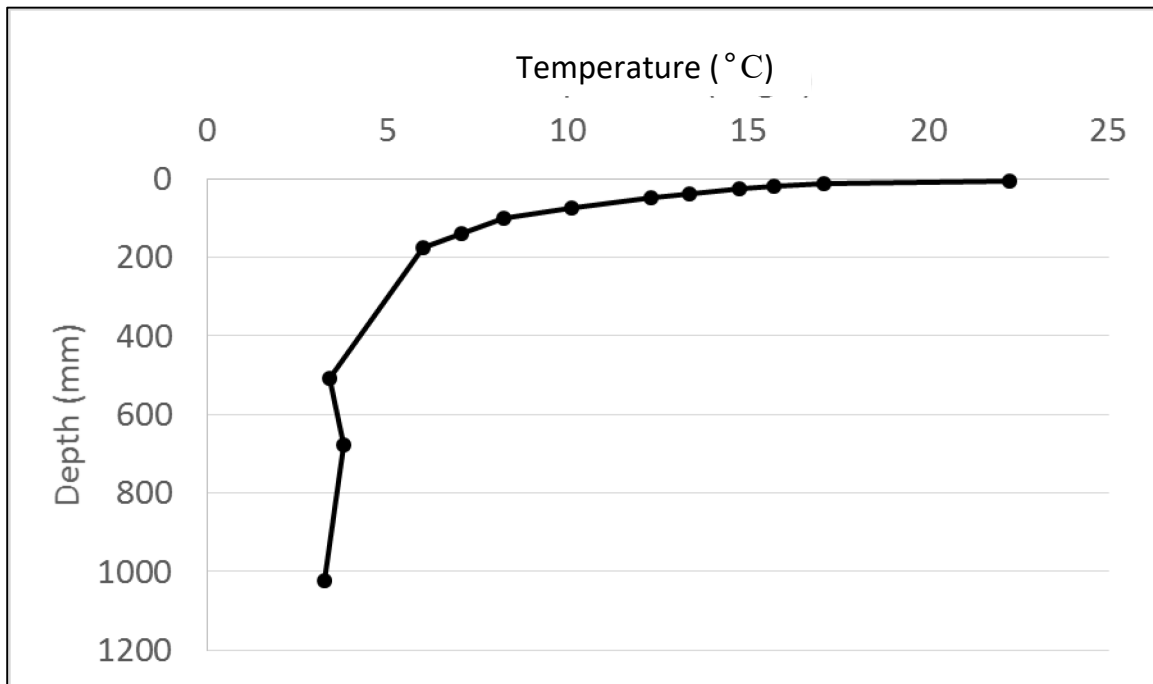


Figure 3.29 Maximum Long-Term Temperature Gradient

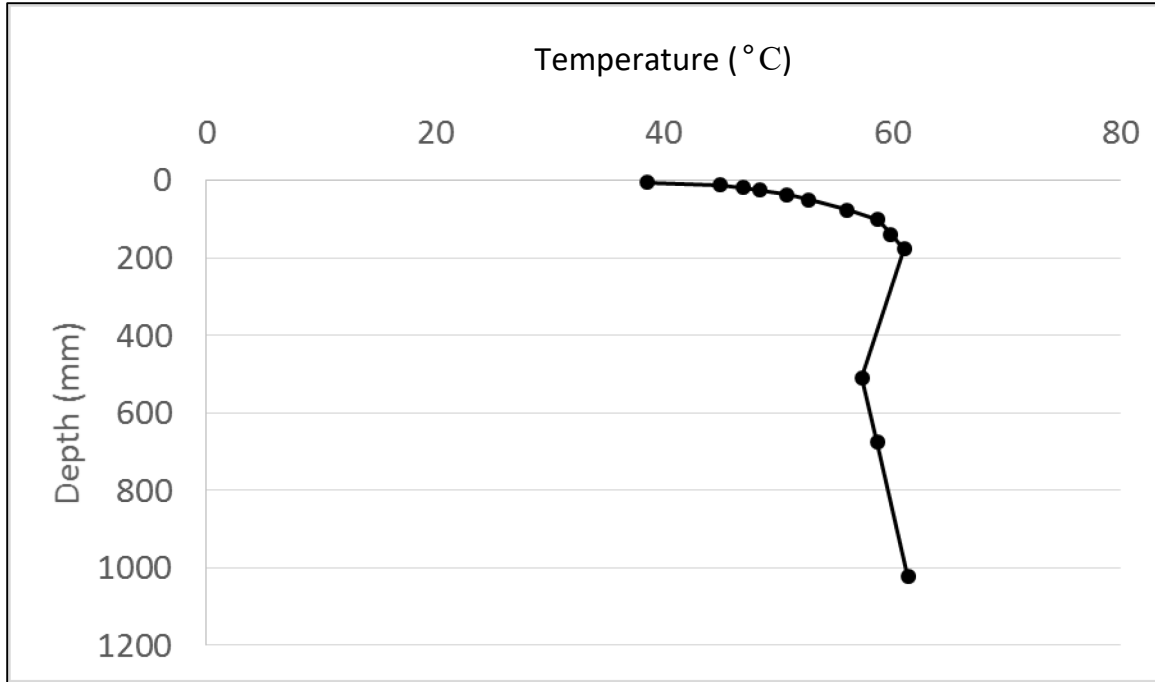


Figure 3.30 Minimum Temperature Gradient during Girder Cooling

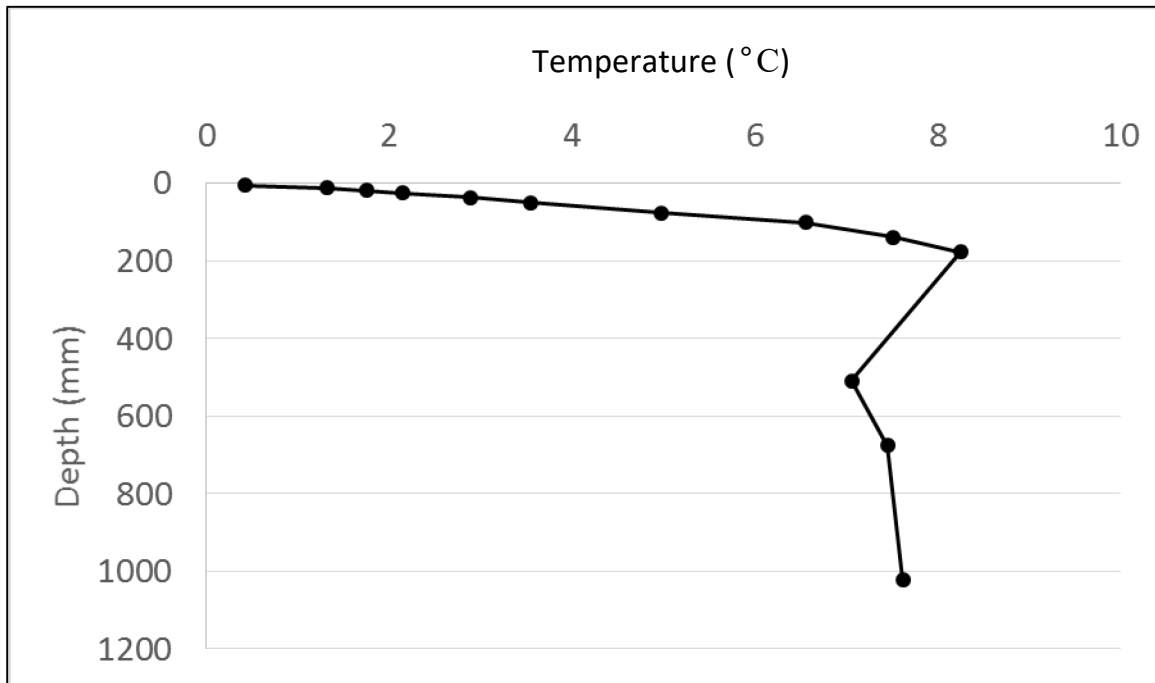


Figure 3.31 Minimum Long-Term Girder Temperature Gradient

3.4.5 Long-Term Temperature Gradients for Site E

Ten thermocouples were placed at Site E—five close to the deck surface and five close to the bottom of the girder. The temperature gradient analyses for Site E were performed similarly to those of other sections, with the exception that thermocouples or vibrating wire strain gauges do not exist at Site E between Thermocouple 5 and the thermocouples at the bottom of the girder. To obtain temperatures at other depths of the girder, temperatures were averaged between sites C and D at the respective depths. These temperature gradients are presented in Figure 3.32 and Figure 3.33. Information about these gradients is presented in Table 3.8.

Table 3.8 Worst Case Temperature Gradient Information for Site E

Analysis	Date	Time	Value of Difference (°C)
Max. 1-UW Difference	2/22/2016	2:30 pm	14.48
Min. 1-UW Difference	12/10/2015	7:15 pm	-4.54

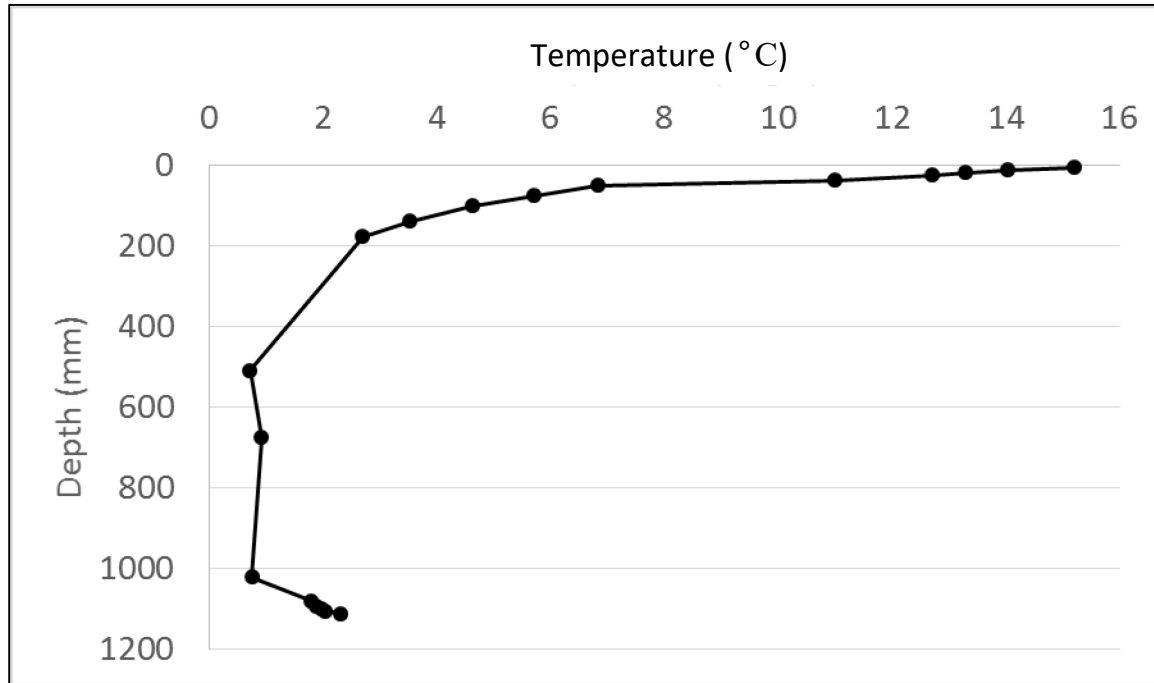


Figure 3.32 Maximum Long-Term Temperature Gradient at Site E

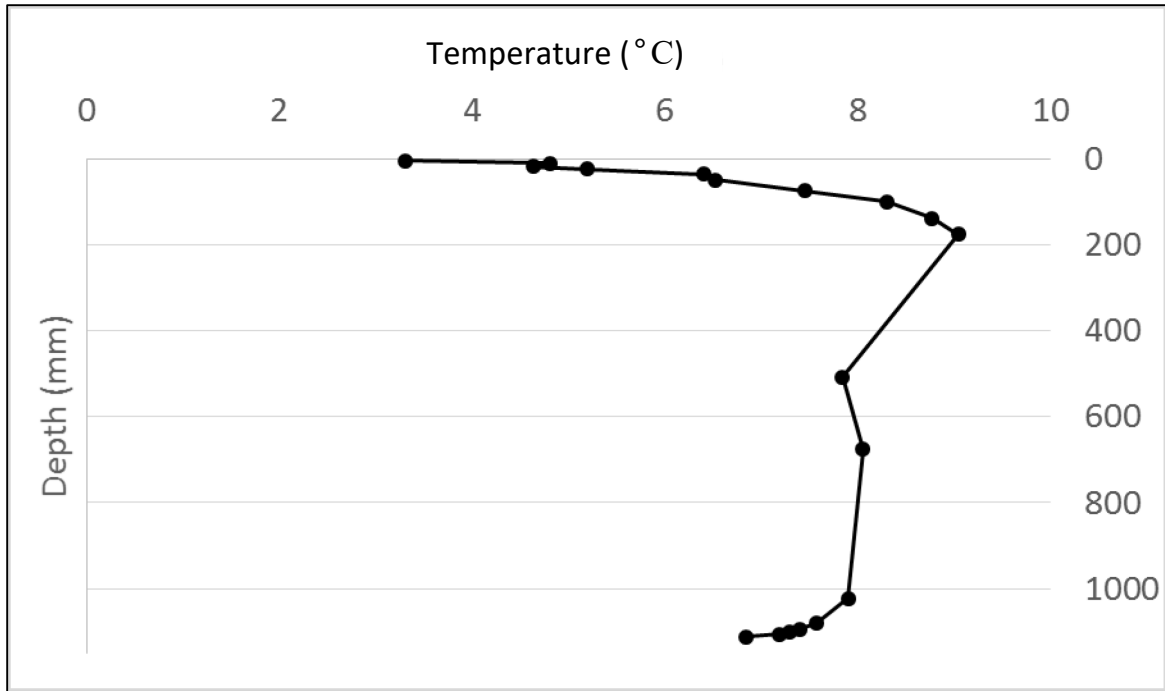


Figure 3.33 Minimum Long-Term Temperature Gradient at Site E

As shown in Figure 3.32 and Figure 3.33, the temperature gradients tend to follow a curved shape. As with the top and bottom of the girder, the web of the girder is more susceptible to temperature change than the thick deck, especially after initially releasing the girder from the concrete forms.

4. COMPARISON WITH PREDICTIVE METHODS

4.1 Description of AASHTO Short-Term Losses

Article 5.9.5.2.3a of the AASHTO LRFD Bridge Design Specifications provides the method for determining the prestress loss due to elastic shortening for pretensioned members. This method for calculating elastic shortening loss is incorporated for both the AASHTO LRFD Refined Method and the AASHTO LRFD Approximate Method discussed in sections 4.2 and 4.3. The code recommended general equation is presented below:

$$\Delta f_{pES} = \frac{E_p}{E_{ct}} f_{cgp} \quad \text{Equation 4.1}$$

Where: Δf_{pES} = change in prestressing steel stress due to elastic shortening; E_p = modulus of elasticity of prestressing steel; E_{ct} = modulus of elasticity of concrete at transfer or time of load application (ksi); f_{cgp} = the concrete stress at the center of gravity of prestressing tendons due to the prestressing force immediately after transfer and the self-weight of the member at the section of maximum moment (ksi). As calculating the elastic shortening prestress loss with Equation 4.1 is an iterative process, the commentary for article 5.9.5.2.3a presents the following alternative equation:

$$\Delta f_{pES} = \frac{A_{ps} f_{pbt} (I_g + e_m^2 A_g) - e_m M_g A_g}{A_{ps} (I_g + e_m^2 A_g) + \frac{A_g I_g E_{ci}}{E_p}} \quad \text{Equation 4.2}$$

Where: A_{ps} = area of the prestressing steel (7.378 in.²); f_{pbt} = stress in prestressing steel immediately prior to transfer (202.63 ksi); I_g = moment of inertia of the gross concrete section (249,031 in.⁴); e_m = average prestressing steel eccentricity at mid-span (22.0 in.); A_g = gross area of section (1107 in.²); M_g = mid-span moment due to member self-weight (12,885 kip-in.); E_{ci} = modulus of elasticity of concrete at transfer (4457 ksi); E_p = modulus of elasticity of prestressing tendons (28,500 ksi).

The modulus of elasticity of the concrete at transfer was calculated using two different methods. The first method is presented in article 5.4.2.4 of the AASHTO LRFD Bridge Design Specifications and is shown as Equation 4.3. The second method is presented in ACI Committee 435 (1995) and is shown as Equation 4.4. The second equation has been shown to more accurately predict the modulus of elasticity for concrete with compressive strengths larger than 41.4 MPa (6,000 psi). Using Equation 4.3, with a w_c value of 137.9 lbs/ft³ for Girder 1 and 139.5 lbs/ft³ for Girder 5, the modulus of elasticity was calculated as 30.63 MPa (4442 ksi). This value was reduced by 9.7% to 27.66 MPa (4011 ksi) when Equation 4.4 was used. The prestress losses using both calculated moduli values were used to calculate the predicted strain losses in Section 4.4.

$$E_c = 33,000 K_1 w_c^{1.5} \sqrt{f_c'} \quad \text{Equation 4.3}$$

$$E_c = \left[40,000 \sqrt{f_c'} + 10^6 \right] \left(\frac{w_c}{145} \right)^{1.5} \quad \text{Equation 4.4}$$

Where: E_c = Concrete modulus of elasticity (ksi for Equation 4.3 and psi for Equation 4.4), K_1 = correction factor for source of aggregate to be taken as 1.0 unless determined by physical test, and as approved by the authority of jurisdiction, w_c = weight of the concrete (kcf for Equation 4.3 and pcf for Equation 4.4), and f_c' = compressive strength of the concrete (ksi for Equation 4.3 and psi for Equation 4.4).

4.2 Description of AASHTO LRFD Long-Term Losses Using the Refined Method

Article 5.9.5.4 of the AASHTO LRFD Bridge Design Specifications provides the recommended method for determining the long-term prestress loss at any time during the service life of a bridge, hereafter known as the Refined Method. The Refined Method is used to determine the long-term losses due to creep, shrinkage, and relaxation of the prestressing strands. The long-term prestress losses are calculated using the general equation provided as Equation 4.5.

$$\Delta f_{pLT} = (\Delta f_{pSR} + \Delta f_{pCR} + \Delta f_{pR1})_{id} + (\Delta f_{pSD} + \Delta f_{pCD} + \Delta f_{pR2} - \Delta f_{pSS})_{df} \quad \text{Equation 4.5}$$

Where: Δf_{pLT} = change in prestressing steel stress due to time-dependent loss; Δf_{pSR} = prestress loss due to shrinkage of girder concrete between transfer and deck placement; Δf_{pCR} = prestress loss due to creep of girder concrete between transfer and deck placement; Δf_{pR1} = prestress loss due to relaxation of prestressing strands between time of transfer and deck placement; Δf_{pR2} = prestress loss due to relaxation of prestressing strands in composite section between time of deck placement and final time; Δf_{pSD} = prestress loss due to shrinkage of girder concrete between time of deck placement and final time; Δf_{pCD} = prestress loss due to creep of girder concrete between time of deck placement and final time; Δf_{pSS} = prestress gain due to shrinkage of deck in composite section; $(\Delta f_{pSR} + \Delta f_{pCR} + \Delta f_{pR1})_{id}$ = sum of time-dependent prestress losses between transfer and deck placement; $(\Delta f_{pSD} + \Delta f_{pCD} + \Delta f_{pR2} - \Delta f_{pSS})_{df}$ = sum of time-dependent prestress losses after deck placement. All variables are measured in ksi.

The bridge for this study was designed and built using a deck bulb tee girder, in which the deck and girder are cast together as one section. Therefore, the $(\Delta f_{pSD} + \Delta f_{pCD} - \Delta f_{pSS})_{df}$ variables all are zero. Below are the equations to estimate the losses due to shrinkage, creep, and relaxation:

$$\Delta f_{pSR} = \varepsilon_{bid} E_p K_{id} \quad \text{Equation 4.6}$$

Where: ε_{bid} = concrete shrinkage strain of girder between the time of transfer and deck placement (varies over time); E_p = modulus of elasticity of prestressing tendons (28,500 ksi); K_{id} = transformed section coefficient that accounts for time-dependent interaction between concrete and bonded steel in the section being considered for the time period between transfer and deck placement (varies over time).

$$\Delta f_{pCR} = \frac{E_p}{E_{ci}} f_{cgp} \Psi_b(t_d, t_i) K_{id} \quad \text{Equation 4.7}$$

Where: E_{ci} = modulus of elasticity of concrete at transfer (4011 ksi using Equation 4.3 and 4442 ksi using Equation 4.4); f_{cgp} = the concrete stress at the center of gravity of prestressing tendons due to the prestressing force immediately after transfer and the self-weight of the member at the section of maximum moment (2,732 psi); $\Psi_b(t_d, t_i)$ = girder creep coefficient at time of deck placement due to loading introduced at transfer (varies over time); Δf_{pR1} and $\Delta f_{pR2} = 1.2$ ksi for low-relaxation strands.

4.3 Description of AASHTO Approximate Method

Article 5.9.5.3 of the AASHTO LRFD Bridge Design Specifications provides an alternative method for estimating the ultimate prestress loss for a typical bridge girder, hereafter known as the Approximate Method. The Approximate Method is used to determine the long-term losses due to creep, shrinkage, and relaxation of the prestressing strands. Given below are the code-presented equations:

$$\Delta f_{pLT} = 10.0 \frac{f_{pi} A_{ps}}{A_g} \gamma_h \gamma_{st} + 12.0 \gamma_h \gamma_{st} + \Delta f_{pR} \quad \text{Equation 4.8}$$

Where:

$$\gamma_h = 1.7 - 0.01H$$

$$\gamma_{st} = \frac{5}{(1 + f_{ci}')$$

Δf_{pLT} = change in prestressing steel stress due to time-dependent loss; f_{pi} = prestressing steel stress immediately prior to transfer (28,500 ksi); A_{ps} = area of the prestressing steel (7.378 in²); A_g = gross area of girder cross section (1107 in²); γ_h = correction factor for relative humidity of the ambient air (1.58); H = the average annual ambient relative humidity (12%); γ_{st} = correction factor for specified concrete strength at time of prestress transfer to the concrete member (0.632); Δf_{pR} = an estimate of relaxation loss taken as 2.4 ksi for low relaxation strand, 10.0 ksi for stress relieved strand and in accordance with manufacturer's recommendation for other types of strand.

4.4 Comparison of Predictive Methods with Measured Losses

4.4.1 Predicted Elastic Shortening Loss Comparison

The predicted elastic shortening loss was estimated using Equation 4.3 and Equation 4.4. The predicted elastic shortening losses were compared against the measured values and are presented in Table 4.1.

Table 4.1 Elastic Shortening Comparison

Girder	Measured Elastic Shortening Loss (ksi)	Calculated Elastic Shortening Loss Using Equation 4.3 (ksi)	Calculated Elastic Shortening Loss Using Equation 4.4 (ksi)	Percent Difference Using Equation 4.3 (%)	Percent Difference Using Equation 4.4 (%)
1	21.65	17.75	19.41	18.0	10.3
5	24.38	17.63	19.22	27.7	21.2

As shown in Table 4.1, predicting elastic shortening using Equation 4.4 produced results closer to the measured results for both girders: 7.7% closer for Girder 1 and 6.5% closer for Girder 5. Interestingly, the percent error associated with the predicted values for Girder 5 was approximately 10% higher than the percent errors for Girder 1.

4.4.2 Predicted Long-Term Losses Using Equation 4.3 Comparison

Predicting losses using Equation 4.3 were compared against the measured losses at the end of the study and are presented in Table 4.2.

Table 4.2 Long-Term Loss Comparison Using Equation 4.3

Girder	Refined Method Predicted Loss Using Equation 4.3 (ksi)	Measured Loss (ksi)	Percent Error (%)
1	40.03	30.44	31.5
5	36.13	40.15	11.1

As shown in Table 4.2, the Refined Method using Equation 4.3 predicted conservative losses at the end of the study by 31.5% and 11.1% for Girder 1 and Girder 5, respectively. The refined method using Equation 4.3 began predicting conservative values of stress after 15 days and 39 days for girders 1 and 5, respectively.

4.4.3 Predicted Long-Term Losses Using Equation 4.4 Comparison

Predicted losses using Equation 4.4 were compared against the measured losses at the end of the study and are presented in Table 4.3.

Table 4.3 Long-Term Loss Comparison Using Equation 4.4

Girder	Refined Method Predicted Loss Using Equation 4.4 (ksi)	Measured Loss (ksi)	Percent Error (%)
1	42.82	30.44	40.7
5	42.84	36.13	18.6

Comparing Table 4.2 and Table 4.3 shows that using Equation 4.4 provides a more conservative long-term prediction. The refined method using Equation 4.4 began predicting conservative values of stress after 12 days and 27 days for girders 1 and 5, respectively. Figure 4.1 presents the comparison of the long-term stress losses. As the graphs of the stress losses using Equation 4.3 and Equation 4.4 produced very similar graphs, only the graph of the predicted stresses using Equation 4.4 are presented in Figure 4.1.

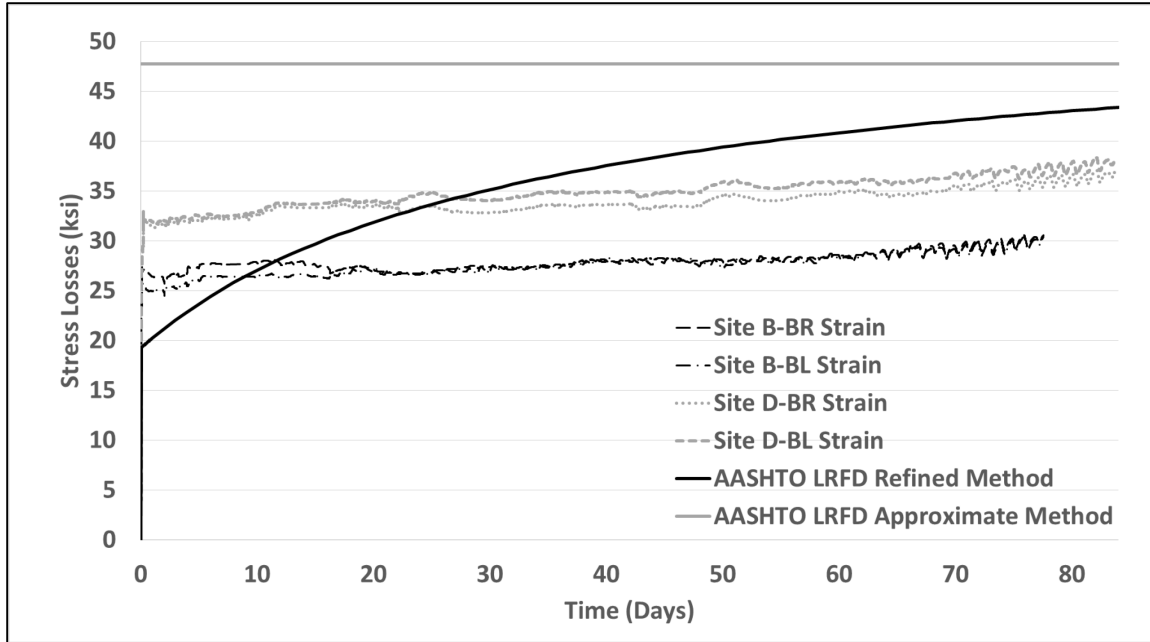


Figure 4.1 Mid-Span Stress Loss Comparisons

Interestingly, the refined method began predicting a more conservative strain loss than the approximate method at 129 days. Therefore, from a design perspective, the refined method is only attractive from 27 to 128 days, as before 27 days the predicted strain may not be conservative and after 128 days the approximate method predicts a strain loss closer to the measured losses.

4.5 Description of AASHTO Temperature Prediction

Article 3.12.3 of the AASHTO LRFD Bridge Design Specifications describes the method for predicting the temperature gradient used for design. This method divides the country into zones. The general shape of the gradient in Figure 3.12.3-2 of the AASHTO LRFD Bridge Design Specifications is presented in Figure 4.2. The zone where the Millville Bridge is built and the type of bridge determines the temperature gradient specifications. T_3 is taken as 0°F unless a site-specific study is performed. Table 4.4 presents the AASHTO temperature gradient specifications for the instrumented bridge. The negative temperature values are obtained by multiplying the positive values by -0.3 for plain concrete decks, which is applicable to this study as the asphalt topping was not placed during this study.

Table 4.4 Bridge Temperature Gradient Specifications

T_1 (°F)	T_2 (°F)	T_3 (°F)	A (in.)
54	14	0	12

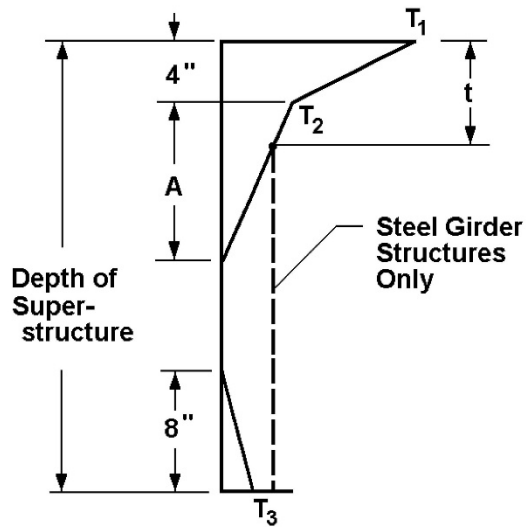


Figure 4.2 3.12.3-2 of the AASHTO LRFD Bridge Design Specifications

4.6 Comparison of AASHTO Temperature Prediction with Measured Temperatures

Figure 4.3 presents the comparison of the AASHTO LRFD temperature gradient prediction method, the Priestley predicted maximum temperature gradient described in Section 2.3, and the maximum measured temperature gradient from Table 3.7. The measured temperatures were translated from their original temperatures to compare against the prediction methods by translating the VWSG temperature at the bottom of the girder to zero degrees Fahrenheit.

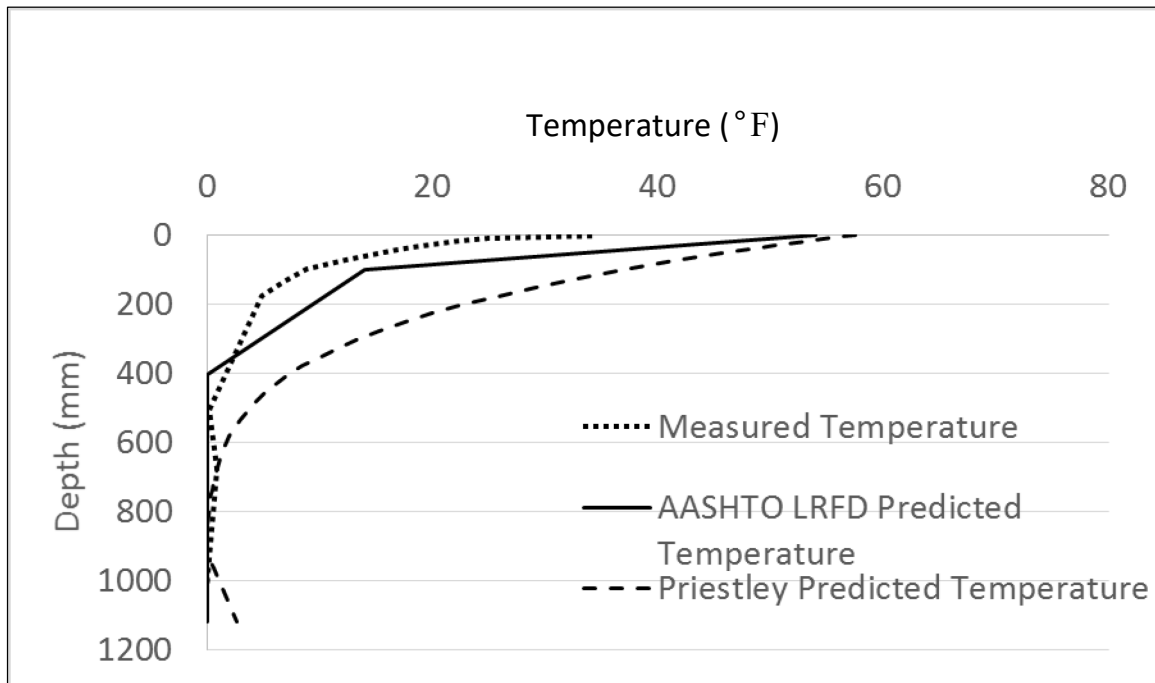


Figure 4.3 Maximum Positive Temperature Gradient Comparison

As can be seen in Figure 4.3, the AASHTO recommended temperature gradient more closely matches the overall shape of the measured temperatures. In comparison, the Priestley method predicts a more gradual temperature change through the bridge superstructure with an increase in temperature occurring at a lower elevation in the girder. However, the code estimated the maximum temperature difference to be much higher than the maximum measured temperature difference of this study. This is to be expected based on the small sample size during the colder winter months during which the data were collected to date. It is anticipated that this difference will be reduced as temperature, which will include the hotter summer months, continues to be recorded. The Priestley predicted gradient calculates the maximum temperature as a function of the blacktop thickness. For no asphalt overlay, the maximum predicted temperature is 32°C and decreases by 0.2°C for every millimeter of asphalt overlay. All these bridge temperatures were recorded without the asphalt overlay on the deck.

The minimum temperature gradient was measured soon after the girder was removed from the casting bed, with the concrete cooling from a high temperature to a low temperature. As the web of the girder gets thinner, the heat dissipates at a faster rate than the thicker concrete sections at the deck and bottom. The minimum temperature gradient was recorded during December.

As with the maximum temperature gradient comparison, the measured temperatures were adjusted for the minimum temperature gradient comparison. The web temperatures were taken as the baseline for comparison with the AASHTO LRFD predicted temperatures. The zero degree measured temperature was taken as thermocouple 10 (bottom of thermocouple bank) as this provided the best comparison against the code estimated temperatures. The minimum temperature gradient (from Table 3.7) was compared against the AASHTO LRFD predicted values and is presented in Figure 4.4.

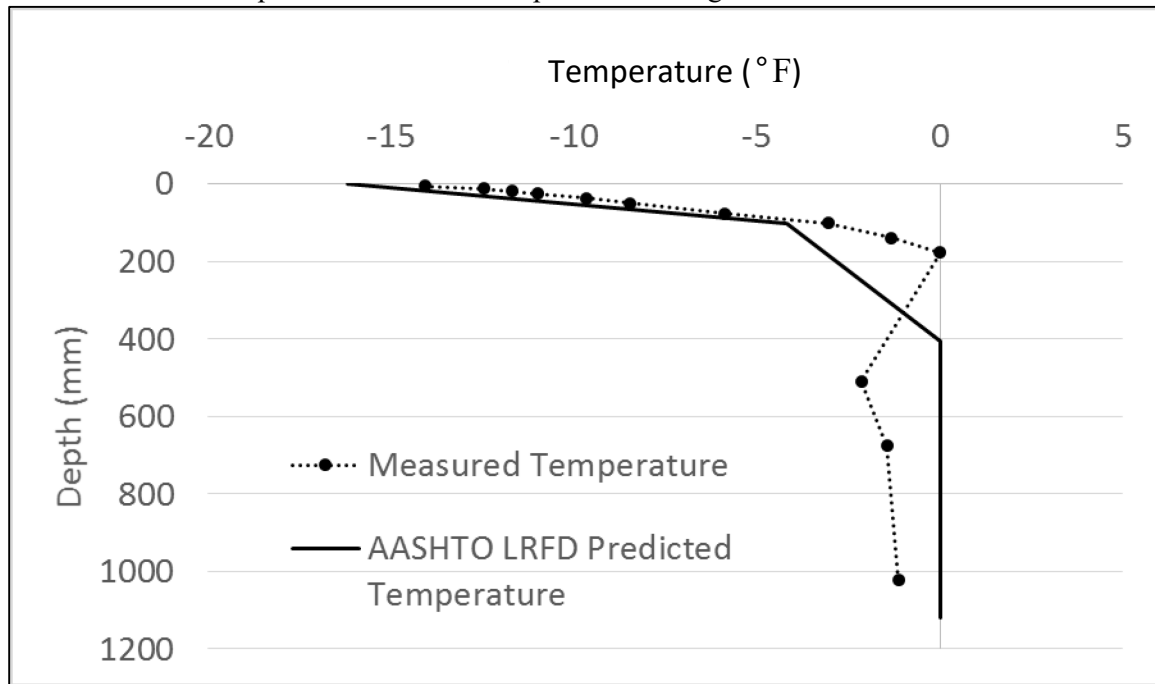


Figure 4.4 Minimum Temperature Gradient Comparison

As shown in Figure 4.4, the minimum measured temperature gradient closely follows the AASHTO LRFD prescribed temperature gradient for the first 100 mm; however, it varies greatly throughout the rest of the bridge superstructure. In this case, the top temperature was within 1.3% of the predicted AASHTO value.

The maximum and minimum temperature gradients at Site E were also analyzed. The comparisons are presented in Figure 4.5 and Figure 4.6. Analysis of the temperature gradient at Site E is advantageous, as the temperatures throughout the girder section can be obtained. However, the maximum and minimum temperature gradients at Site E may not be a representation of the absolute maximum and minimum temperature gradients.

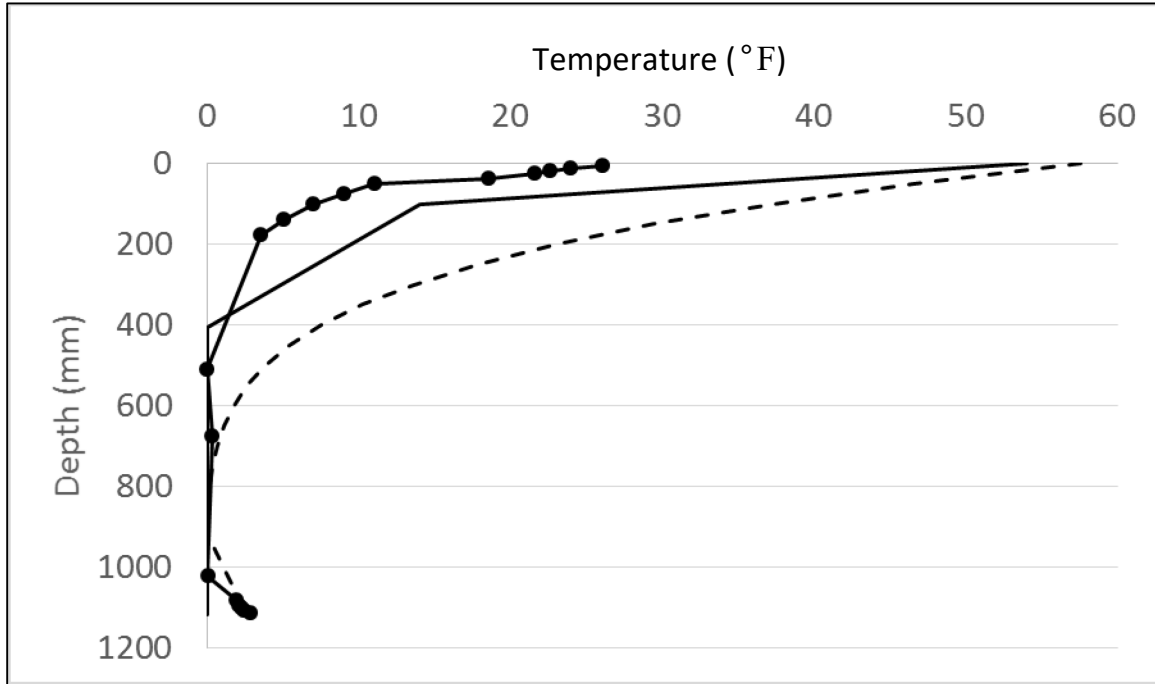


Figure 4.5: Site E Maximum Temperature Gradient Comparison

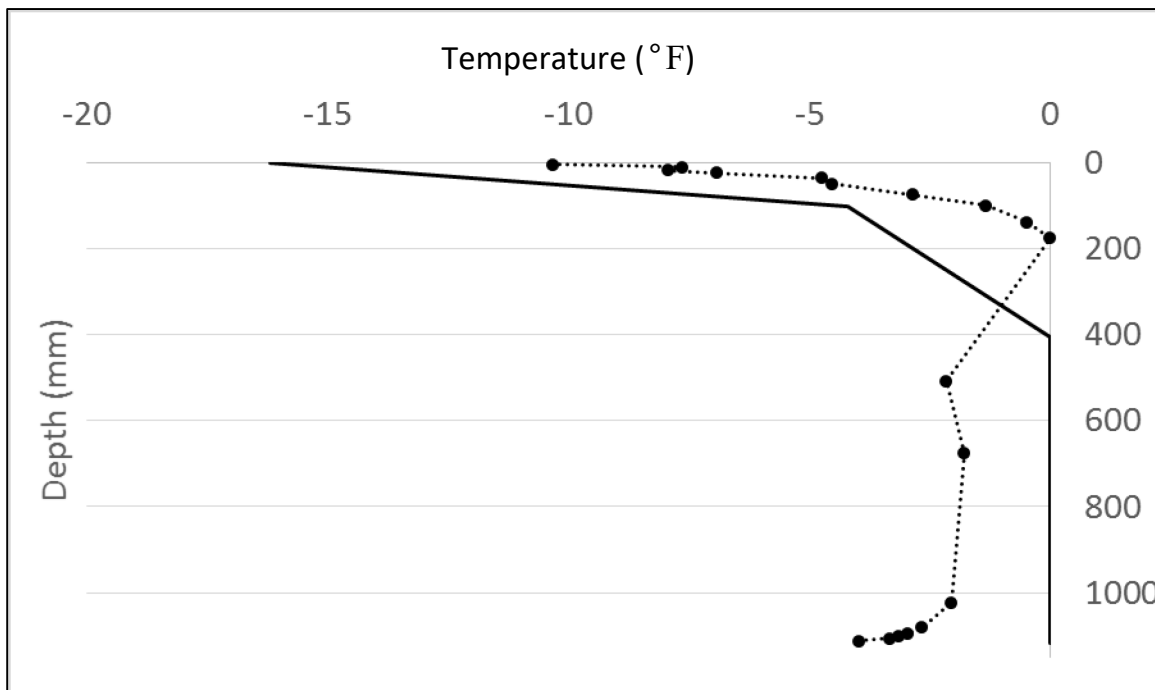


Figure 4.6 Site E Minimum Temperature Gradient Comparison

As shown in Figure 4.5, the maximum temperature difference for Site E was 76.9% lower than the AASHTO LRFD predicted difference. However, the slope of the temperature gradient close to the deck surface was similar to the AASHTO LRFD predicted temperature gradient slope. Also, at the bottom of the girder, the temperatures closely followed the Priestley predicted temperatures.

As shown in Figure 4.6, the minimum temperature gradient curve for Site E followed the AASHTO LRFD curve, albeit with higher values, for the first 100 mm. The percent difference of the predicted and measured temperature at the deck surface was 76.9%. At depths lower than 100 mm, the AASHTO LRFD Bridge Design Specifications poorly predicts the shape of the temperature gradient curve. The lower portions of the girder showed more susceptibility to the cooling temperatures than the thick upper portion.

5. SUMMARY AND THESIS

5.1 Summary

The Millville Bridge was constructed as a deck bulb tee girder bridge. The bridge spans the Blacksmith Fork River and provides access to the Ridgeline High School in Millville, Utah. The girders were fabricated using precast, prestressed concrete. The bridge girders were fabricated in December 2015 and shipped to the site in January 2016. The construction was completed over the next several months and was open to traffic in August 2016. The bridge was designed using a single 90-ft. span and was designed to carry two lanes of traffic.

The Utah Transportation Center (UTC), in partnership with the Mountain Plains Consortium, sponsored a study to investigate the changes in prestress and temperature for the Millville Bridge over the Blacksmith Fork River. To accomplish the goals of the study, the bridge was instrumented with 16 vibrating wire strain gauges located at four cross-sections. An additional 50 thermocouples at five cross-sections were installed. Four of the thermocouple locations are at the same locations as the vibrating wire strain gauges. These instrument locations were placed at the mid-span and end of an exterior and center girder to effectively measure the bridge response in one quarter of the bridge superstructure. These instruments were tied to the reinforcing steel before the concrete was poured at the precast plant.

For the prestress loss analysis, four vibrating wire strain gauges were placed at four different bridge locations, with one placed in the upper web, one in the lower web, and two at the center of the prestressing strands in the bottom of the girder. The change in strain measurements were recorded beginning immediately prior to the releasing of the prestressing strands. The average change in strain at the centroid of the prestressing strands for the two vibrating wire strain gauges at mid-span were used to determine the change in prestress. These recorded measurements were compared with calculated values using the Approximate and Refined Methods provided in the AASHTO LRFD Bridge Design Specifications.

For the temperature portion of the study, ten thermocouples were placed at five different bridge locations. Four of the locations supplemented readings measured by thermistors in the strain gauges and consisted of 10 gauges in the top of the deck. At the fifth location, five thermocouples were placed at the top and bottom of the girder. Temperature data and gradients were recorded and analyzed during and after concrete curing. The maximum and minimum long-term temperature gradients were compared against the design gradients provided in the AASHTO LRFD Bridge Design Specifications.

5.2 Conclusions

Measured prestress losses using readings from the internally installed vibrating wire strain gauges were analyzed and compared against the AASHTO LRFD Bridge Design Specifications. Additionally, temperature gradients during and after curing were measured and compared with gradients recommended in the AASHTO LRFD Bridge Design Specifications. Based on the findings of this research, several conclusions were formed.

- The measured elastic shortening losses were compared with calculated values using relationships presented in the AASHTO LRFD Bridge Design Specifications (Equation 4.3) and the ACI Committee 435 (1995) specified equation (Equation 4.4) for modulus of elasticity. It was concluded that for this bridge, the elastic shortening calculated using the ACI equation for modulus of elasticity of high strength concrete more closely predicts the measured response of the bridge than using the AASHTO equation for modulus of elasticity. The percent errors for the

AASHTO equation were 18.0% and 27.7% for Girder 1 and Girder 5, respectively. The percent errors for the ACI equation were 10.3% and 21.2% for Girder 1 and Girder 5, respectively.

- Over the long term, the measured prestress losses followed a nearly linearly increasing relationship during the course of this study, with higher daily fluctuations as the ambient temperature increased in the spring. The total percent loss of the jacking stress at the end of the study was 15.0% and 17.8% for Girder 1 and Girder 5, respectively.
- Comparing the measured prestress losses against the prestress losses predicted with the AASHTO LRFD Approximate and Refined methods proved conservative over the long-term analysis of this study. However, the refined method predicted prestress losses that were unconservative for approximately the first month after the release of the prestressing strands and then became conservative over the rest of the recorded period. The results of the measured losses against the Refined and Approximate methods using the AASHTO and ACI equations for modulus of elasticity are given in Table 5.1.

Table 5.1 Long-Term Percent Errors of Refined and Approximate Methods Using AASHTO and ACI Modulus of Elasticity Equations

Girder	Refined Method Using AASHTO Percent Error	Refined Method Using ACI Percent Error	Approximate Method Using AASHTO Percent Error	Approximate Method Using ACI Percent Error
1	31.5	40.7	51.5	56.8
5	11.1	18.7	27.7	32.1

- The temperature gradients predicted with the AASHTO LRFD Bridge Design Specifications proved to be conservative over the length of this study. As the length of the study was approximately three months, it is assumed that the measured temperature gradients will likely be closer to the design temperature gradients. The percent errors for the temperature gradient comparisons for this study were 58.0% and 1.3% for the maximum and minimum temperature gradients, respectively.

5.3 Recommendations for Additional Research

Additional research is needed to influence the AASHTO LRFD Bridge Design Specifications for prestress loss predictions, specifically in regard to the modulus of elasticity predictions and the Refined Method for predicting long-term prestress losses. Additionally, more research should be performed to quantify the differences in measured prestress losses as impacted by differences in curing of Girder 1 and Girder 5. Lastly, more research should be performed to better understand the temperature gradient fluctuations for all depths of the bridge superstructure, specifically in the web during cooling.

BIBLIOGRAPHY

American Association of State Highway and Transportation Officials (AASHTO). (2010). *AASHTO LRFD Bridge Design Specifications*. Washington, D.C.: American Association of State Highway and Transportation Officials (AASHTO).

American Concrete Institute (ACI). (1995). *ACI Committee 435*. Section 2.3.2.

Barr, P., Kukay, B., and Halling, M. (2008). "Comparison of Prestress Losses for a Prestressed Concrete Bridge Made with High-Performance Concrete." *New Horizons and Better Practices*: pp. 1-8.

Saiidi, M., Hutchens, E., and Gardella, D. (1998). "Bridge Prestress Losses in Dry Climate." *Journal of Bridge Engineering*, 10.1061/(ASCE)1084-0702(1998)3:3(111), 111-116.

Priestley, M. (1978). "Design of Concrete Bridges for Temperature Gradients." *American Concrete Institute (ACI) Journal*, 75(23), 209-217.

Rodriguez, L., Barr, P., and Halling, M. (2014). "Temperature Effects on a Box-Girder Intermittent Abutment Bridge." *Journal of Performance of Constructed Facilities*, 10.1061/(ASCE)CF.1943-5437, 583-591.

Roberts-Wollman, C., Breen, J., and Cawrse, J. (2002). "Measurements of Thermal Gradients and their Effects on Segmental Concrete Bridge." *Journal of Bridge Engineering*, 10.1061/(ASCE)1084-0702(2002)7:3(166), 166-174.

APPENDIX A

Appendix A provides the initial strain loss figures for Girder 5.
Girder 5 Initial Strain Losses

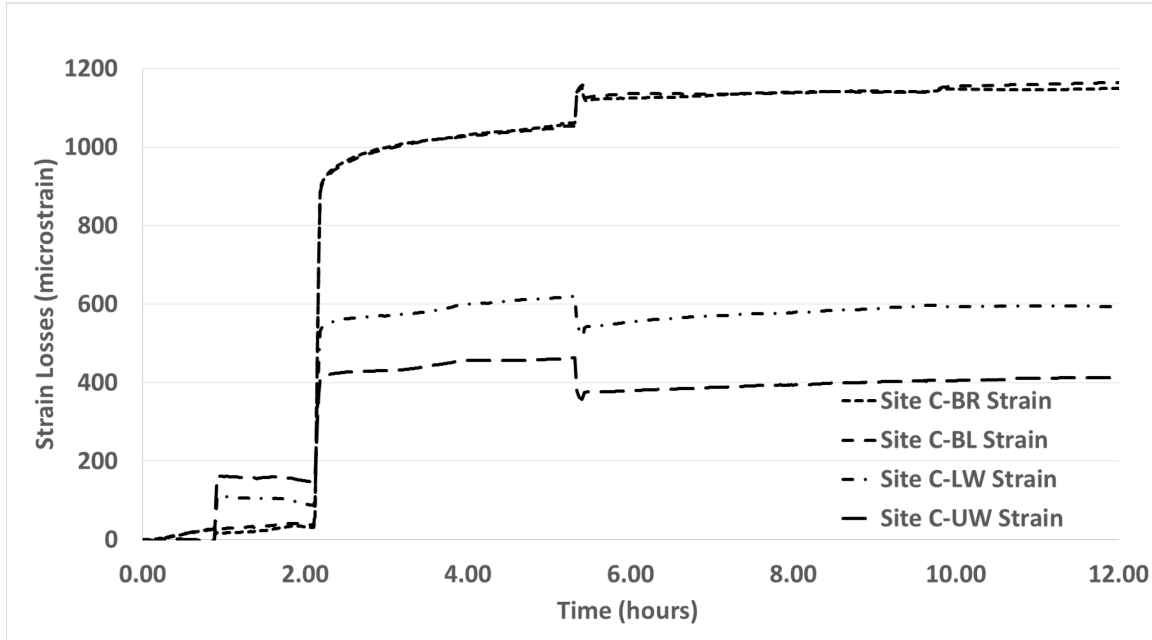


Figure A.1 Initial Girder Destressing Strain Losses for Site C

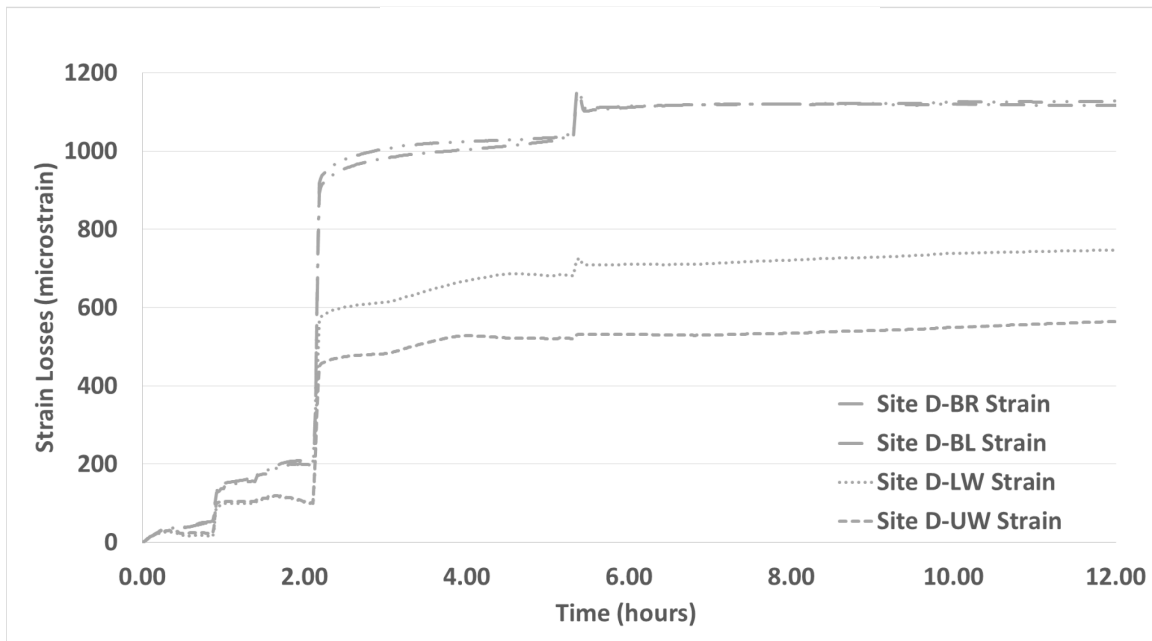


Figure A.2 Initial Girder Destressing Strain Losses for Site D